

1 **Meta-analytical insights into organic matter enrichment in the surface** 2 **microlayer**

3 Amavi Silva¹, Surandokht Nikzad^{2,3}, Theresa Barthelmeß¹, Anja Engel¹, Hartmut Herrmann⁴, Manuela
4 van Pinxteren⁴, Kai Wirtz^{3,5}, Oliver Wurl⁶ and Markus Schartau¹

5 ¹GEOMAR Helmholtz Centre for Ocean Research Kiel, Kiel, 24143, Germany

6 ²Trent University, Peterborough, ON K9L 0G2, Canada

7 ³Institute of Coastal Systems, Helmholtz-Zentrum Hereon, Geesthacht, 21502, Germany

8 ⁴Leibniz Institute for Tropospheric Research (TROPOS), Atmospheric Chemistry Department (ACD), Leipzig, 04318,
9 Germany

10 ⁵Christian-Albrechts University of Kiel, Kiel, 24148, Germany

11 ⁶Carl von Ossietzky University of Oldenburg, Oldenburg, 26129, Germany

12 Correspondence to: Amavi Silva (asilva@geomar.de), Markus Schartau (mschartau@geomar.de)

13 **Abstract.** The surface microlayer (SML), the uppermost ~1 mm water layer at the air-water interface, plays a critical role in
14 mediating Earth system processes, yet current knowledge of its composition and organic matter enrichment remains scattered
15 across disciplines. Here, we present the first known meta-analysis of SML studies that quantitatively assesses the distributional
16 characteristics of selected organic compounds, including organic carbon and nitrogen, amino acids, fatty acids, transparent
17 exopolymer particles, carbohydrates, lipids and proteins, through probability density estimates, central tendency metrics and
18 correlation analyses. Our results confirm a preferential enrichment of nitrogen-enriched, particulate organic matter in the SML,
19 while also highlighting the significance of surfactant-specific factors that govern selective enrichment in the SML. We find
20 that enrichment patterns can vary systematically with environmental and methodological conditions, underscoring the need to
21 account for such influences when interpreting observations and developing SML-based models. We provide the full range of
22 typical EF values for the studied compounds, offering a clear reference for assessing whether new measurements are typical
23 or extreme. While delving into the ability of EFs to reflect organic matter partitioning in the SML, we also critically examine
24 their limitations in capturing trophic variability and suggest that EF-based assessments be complemented with metrics that
25 remove background variability from underlying water concentrations, enabling more accurate interpretations of true SML
26 enrichment and informing future modelling efforts. Additionally, our meta-analysis demonstrates that logarithmic data
27 transformations and robust central tendency estimates outperform traditional linear-scale approaches, providing more accurate
28 and reliable SML enrichment estimates.

29 **1 Introduction**

30 Approximately 70% of the Earth's surface is covered by a hydrated gelatinous 'skin' known as the surface microlayer
31 (hereafter referred to as 'SML'; note that while this term is commonly used to denote the sea surface microlayer, in this study

32 it refers to the surface microlayer in both marine and freshwater systems), which has an operationally defined thickness
33 typically ranging from 1 – 1000 μm , depending on the sampling method used (i.e., screen, plate, drum: Astrahan et al., 2016;
34 Hunter, 1980; Liss and Duce, 1997; Wurl et al., 2009). Situated between the surface waters of all natural water bodies and the
35 atmosphere, this uppermost multi-component layer (Astrahan et al., 2016; Carlucci et al., 1985; Cunliffe et al., 2013) creates
36 a unique microhabitat, mainly consisting of neuston (i.e., living communities in the SML), a relatively enriched complex of
37 organic compounds and strong physico-chemical gradients (Cunliffe et al., 2013; Dietz et al., 1976; Engel and Galgani, 2016;
38 Hunter and Liss, 1977). The formation and the composition of the SML are governed by a number of biological, physical and
39 chemical drivers that interact under varying complex environmental conditions and time scales. As a result, the SML dynamics
40 play a pivotal role in a range of environmental processes such as air-water gas exchange, heat transfer across boundary layers,
41 biogeochemical cycling, microbial interactions and distribution of pollutants (e.g., Engel et al., 2017; Frew, 1997; Liss and
42 Duce, 1997; Upstill-Goddard, 2006). Therefore, continued investigation of the compositional heterogeneity of the SML and
43 of the processes therein is crucial to gain deeper insights into its role in ocean biogeochemistry and its potential climate
44 interactions.

45 The SML is shaped by physical forces: surface tension provides structural stability at the air-water interface (Liss and Duce,
46 1997), while diffusive fluxes, bubble scavenging and the upward transport of buoyant particles deliver material from
47 underlying waters (hereafter referred to as ‘ULW’; Baastrup-Spohr and Staehr, 2009; Chen et al., 2016; Joux et al., 2006;
48 Obernosterer et al., 2005). In addition, wet and dry atmospheric deposition as well as in situ production and degradation also
49 lead to concentration changes in the SML (Astrahan et al., 2016; Kuznetsova et al., 2004; Milinković et al., 2022). Within the
50 SML, biological and chemical processes continuously transform compounds between dissolved and particulate forms (Liss
51 and Duce, 1997), further contributing to its characteristic enrichment relative to the ULW (e.g., Baastrup-Spohr and Staehr,
52 2009; Gao et al., 2012; Gašparović et al., 2007; Liss and Duce, 1997; Marty and Saliot, 1976; Yang, 1999).

53 Many compounds present in the SML are surface active and are collectively known as ‘surface-active agents’ or ‘surfactants’
54 (Maki and Hermansson, 2020; Wurl and Holmes, 2008). Surfactants tend to adsorb at the air-water interface (Wurl et al., 2009)
55 due to their amphiphilic nature (i.e., presence of both hydrophobic and hydrophilic structural parts; e.g., Marty and Saliot,
56 1976) and form interfacial films. This leads to modifications of the physico-chemical characteristics of the sea surface, most
57 notably surface tension, elasticity and viscosity, which alter momentum transfer, micro-scale wave breaking, damping of
58 capillary waves, ultimately affecting air-sea gas exchange (McKenna and McGillis, 2004; Pereira et al., 2016). Selective
59 enrichment of surfactants in the SML is strongly influenced by phytoneuston exudation and grazing processes (Kujawinski et
60 al., 2002; Žutić et al., 1981), which release carbohydrates that constitute a major fraction of naturally occurring biosurfactants
61 (Myklestad, 1995; Penna, 1999). Blooms facilitate the accumulation of large hydrophilic polysaccharides, which can bind to
62 hydrophobic groups and thereby acquire surfactant properties (Wurl et al., 2011). Surfactant distribution is further shaped by
63 microbial activity (Hunter and Liss, 1977; Kurata et al., 2016); Baceterioneuston is predominantly lipolytic and proteolytic,

64 breaking down organic matter (OM) into lipids and proteins (polymers of amino acids; Carlucci et al., 1985; Kjelleberg et al.,
65 1976; Sieburth et al., 1976), both of which represent abundant biosurfactant pools in the SML (Brinis et al., 2004; Marty and
66 Saliot, 1976). However, carbohydrates and polysaccharides also constitute major, rapidly utilized substrates for heterotrophic
67 bacteria in the SML (Harvey et al., 1995; Penezić et al., 2022).

68 Surfactants have been categorized according to their solubility into dry and wet surfactants, of which the more insoluble
69 fraction tends to establish as a monolayer at the surface (e.g., phospholipid-like material; Frka et al., 2012), while the adsorption
70 of the latter fraction (more soluble; e.g., proteins and carbohydrates) is governed by concentration-driven equilibria
71 (Asmussen-Schäfer et al., 2026; Laß and Friedrichs, 2011). Nonetheless, the natural soluble surfactant pool frequently reaches
72 a threshold beyond which monolayer-like surfactant coverage of the air–sea interface is observed (Asmussen-Schäfer et al.,
73 2026). In addition to their chemical composition, surfactants also vary in their size: Colloidal and particulate organic matter
74 accumulated in the SML further provide substrates to bacterioneuston, thereby helping to stabilize the surface films (Sieburth,
75 1983). The contribution from the particulate pool to the SML’s surface activity is estimated to range from 10% to 55%
76 (Gašparović and Čosović, 2003). Furthermore, sticky microgels, like transparent exopolymer particles (TEP) that originate
77 from bacteria and phytoplankton (Alldredge et al., 1993), are also found in the SML. Such gel-like particles can form through
78 the coagulation of dissolved polysaccharides (Engel et al., 2004; Mari and Burd, 1998; Schartau et al., 2007), and are capable
79 of incorporating other compounds into a cohesive matrix (Cunliffe et al., 2009; Sieburth, 1983; Wurl and Holmes, 2008),
80 thereby enhancing the structural integrity of surface films (Cunliffe and Murrell, 2009). When the SML becomes highly
81 concentrated in surfactants, these films transform into thick surface slicks that are visible to the naked eye (Liss and Duce,
82 1997). The extent to which OM-driven changes in SML surfactant composition alter air-sea gas exchange remains to be fully
83 understood (Pogorzelski et al., 2006). In addition, inorganic ions, which do not preferentially adsorb at the air-water interface,
84 can be also present in the SML due to passive upward transport (Knipping et al., 2000; Petersen et al., 2004).

85 Liss and Duce (1997) and Pereira et al. (2018) argue that the SML can restrict diffusive fluxes across the air-sea interface,
86 substantially contributing to reduced rates of ocean-atmosphere gas exchange. Surfactants can impact air-sea gas exchange of
87 greenhouse gases such as carbon dioxide (CO₂), methane (CH₄), nitrous oxide (N₂O) and dimethyl sulfide (DMS) (Frew, 1997;
88 Upstill-Goddard, 2006). Asher (1997), from laboratory measurements, and Tsai and Liu (2003), from global ocean
89 observations, estimate a reduction of annual net CO₂ flux by ~20% – 50% due to the presence of the SML, while Wurl et al.
90 (2016), from in situ measurements, propose that this decrease can be ~15%. Barthelmeß et al. (2021) observed that, in a newly
91 upwelled filament off Mauritania, surfactants can suppress CO₂ gas exchange by 12%. Both lab- and field-based experiments
92 find that natural slicks can reduce air-sea gas exchange by 50 – 60% (Goldman et al., 1988; Salter et al., 2011; Mustaffa et al.,
93 2020), causing the SML to drive an overall reduction of 19% in the CO₂ fluxes, as shown by in situ observations (Mustaffa et
94 al., 2020). Supporting earlier findings of Springer and Pigford (1970), McKenna and McGillis (2004) and Sabbaghzadeh et al.
95 (2017), who raised concerns about the impact of the SML’s surfactants on uncertainties in air-sea gas exchange models,

96 Mustaffa et al. (2020) further argue that conventional wind-based models miscalculate CO₂ exchange up to 20% in areas with
97 high surfactant concentrations. Moreover, Kock et al. (2012) find that, in the eastern tropical North Atlantic region, offsets
98 between air-sea and diapycnal N₂O fluxes could be explained when surfactant effects were introduced to gas exchange models.
99 Work of Goldman et al. (1988) find that surfactants in the SML can also suppress air-sea gas exchange of oxygen (O₂).
100 Disparities in these studies emphasize the significance of accurately assessing the characteristics of the SML and its processes,
101 as well as integrating this knowledge into climate relevant ocean-atmosphere models (Milinković et al., 2022) in order to
102 reduce uncertainties in global gas flux estimations, particularly given that SML is seldom included in gas exchange models
103 (Cen-Lin and Tzung-May, 2013; Engel et al., 2017).

104 Although the composition and the concentration of compounds within the SML are thought to be strongly correlated with those
105 of the ULW (Baastrup-Spohr and Staehr, 2009; Chen et al., 2016; Joux et al., 2006; Kuznetsova et al., 2004), certain substances
106 are selectively accumulated at the air-water interface, leading to a pronounced enrichment in the SML. Several studies,
107 including (Carlucci et al., 1985; Henrichs and Williams, 1985; Kuznetsova and Lee, 2002; Reinthaler et al., 2008), find stronger
108 enrichment of particulate fractions and nitrogen-based compounds compared to dissolved organic carbon. The accumulation
109 of these specific compounds in the SML relative to the ULW is often described by the ‘Enrichment Factor’ (hereafter referred
110 to as ‘EF’). The EF of a compound ‘x’ is given by the following concentration ratio:

$$111 \quad \text{EF of } x = \frac{\text{Concentration of } x \text{ in SML}}{\text{Concentration of } x \text{ in ULW}} \quad (1)$$

112 According to this equation, when the concentration of x is higher in the SML than in the ULW, the EF value rises above 1;
113 when it is lower, the EF drops below 1, as discussed in Carlson (1983) and Garabetian et al. (1993). However, previous studies
114 report substantial enrichment variability in the SML across environments, compound classes and spatio-temporal scales. For
115 instance, non-slick areas where microbial degradation processes are dominant can also demonstrate higher EF values,
116 resembling those found in slick conditions (e.g., Baastrup-Spohr and Staehr, 2009). In contrast, some lakes appear to exhibit
117 weak SML enrichment even under eutrophic ULW conditions when the waters are concentrated by autochthonous OM (i.e.,
118 originate within the same ecosystem they are found) that show a lower affinity to the air-water interface (Hillbricht-Ilkowska
119 and Kostrzewska-Szlakowska, 2004). Freshwater SML tends to be more enriched with organic carbon and nitrogen, total
120 phosphorous, ammonia and phosphate ions (Knulst et al., 1997; Münster et al., 1998; Södergren, 1987), whereas in marine
121 environments, carbohydrates, lipids, proteins and amino acids tend to be more enriched (Liss and Duce, 1997). Concentration
122 variability of the SML can be significantly larger than that of the ULW (Reinthaler et al., 2008), although in some occasions,
123 the two layers show similar variability (Carlson, 1983). Likewise, the extent to which SML composition mirrors the ULW also
124 varies, with some studies observing tight coupling (e.g., Chen et al., 2016; Joux et al., 2006) and others reporting marked
125 decoupling linked to different mineralization rates or adsorption dynamics (e.g., Kuznetsova et al., 2004). Differing surface

126 activities (i.e., tendency of a substance to accumulate at the interface) of organic compounds is considered a major driver of
127 these transfer dynamics between the SML and the ULW (Engel et al., 2017). Environmental factors further influence SML
128 enrichment, yet their influence remains inconsistent and unresolved (e.g., Baastrup-Spohr and Staehr, 2009; Carlson, 1983;
129 Reinthaler et al., 2008; Sabbaghzadeh et al., 2017). Collectively, these heterogeneous findings highlight the complexity of SML
130 enrichment processes and the need for systematic cross-study evaluations. These aspects and their implications are further
131 discussed in the Discussion.

132 Overall, the diversity of reported findings highlights the need for a more holistic view of the applicability of EF as a valid and
133 meaningful indicator of compounds enriched in the SML. To address this, we adopted a meta-analysis of existing SML studies,
134 and conducted a comprehensive analysis to (1) assess OM enrichment in the SML, (2) review current EF estimates and (3)
135 investigate the relevance of EF values as accurate indicators of OM enrichment. The data collection presented here covers
136 mass concentrations of OM compounds and does not include measurements of surface activities or effects on the physico-
137 chemical properties of the uppermost monolayer of the SML. The primary objective is to provide an overview and specific
138 insights into OM compounds that can accumulate within the SML and potentially be linked to biogeochemical processes
139 occurring in the ULW. Accordingly, surfactant measurements of surface activities that have been converted into equivalent
140 surfactant concentrations, such as those expressed as Triton X-100 equivalents, are not considered here. Ultimately, this data
141 compilation, together with the knowledge derived from its initial meta-analysis, is intended to establish a robust foundation
142 for subsequent studies that may support future modelling efforts linking biological processes to functions of the SML and their
143 implications for biogeochemistry and climate.

144 **2 Methodology**

145 The work presented here synthesizes findings from multiple studies on the SML and employs a quantitative meta-analysis.
146 Meta-analyses provide an essential means of extracting robust and generalizable conclusions by integrating results from
147 fragmented bodies of literature. Such systematic reviews can provide a more precise and accurate understanding of overarching
148 trends, even when individual studies report inconsistent results (Crocetti, 2016). Mengist et al. (2020) highlight the importance
149 of meta-analyses by stating that “*Systematic reviews with meta-analysis represent the gold standard for conducting reliable
150 and transparent reviews of literature.*” In fields such as SML research, where methodological diversity is high and
151 environmental variability is inherent, meta-analytical approaches are invaluable in identifying coherent trends and key
152 constraints.

153 **2.1 Data collection and compilation**

154 The primary dataset consists of 2055 data points, extracted from 31 peer-reviewed publications (hereafter referred to as
155 ‘reference studies’) identified through a comprehensive and systematic literature search of scholarly articles published between

156 1967 and 2022. These studies were identified through a structured Google Scholar search conducted between February 2025
157 to April 2025. Search terms included combinations of descriptors related to the surface microlayer (e.g., ‘sea surface
158 microlayer’, ‘SML’), enrichment terminology (e.g., ‘enrichment’, ‘enrichment factor’), and compound specific keywords (e.g.,
159 ‘surfactants’, ‘organic carbon’, ‘organic nitrogen’, ‘TEP’, ‘Amino acids’, and other organic matter classes). Additional relevant
160 publications were identified through reference lists of retrieved papers. Only datasets providing extractable numerical values
161 were retained.

162 From these studies, directly measured mass concentration data were extracted from simultaneously collected SML and ULW
163 samples (hereafter referred to as $[C]_{\text{SML}}$ and $[C]_{\text{ULW}}$, respectively) for twelve different observational types of organic
164 compounds (hereafter known as ‘target compounds’): total organic carbon (TOC expressed in mg L^{-1}), particulate organic
165 carbon (POC in mg L^{-1}), dissolved organic carbon (DOC in mg L^{-1}), total organic nitrogen (TON in mg L^{-1}), particulate organic
166 nitrogen (PON in mg L^{-1}), dissolved organic nitrogen (DON in mg L^{-1}), amino acids (AA in $\mu\text{mol L}^{-1}$), fatty acids (FA in μg
167 L^{-1}), transparent exopolymer particles (TEP in $\mu\text{g Xeq L}^{-1}$), carbohydrates (CHO in $\mu\text{mol L}^{-1}$), lipids (in $\mu\text{mol L}^{-1}$) and proteins
168 (in $\mu\text{mol L}^{-1}$). TOC pool includes all forms of organic carbon, thus comprising both POC and DOC. Similarly, the TON pool
169 combines both PON and DON. In general, the particulate pool constitutes a minor fraction of the total pool. The major classes
170 of biopolymers are proteins, CHO and lipids, with AA serving as the monomers of proteins. Depending on the elemental
171 composition of these biopolymers, they contribute to both, the organic carbon and/or organic nitrogen pool. While the ratio of
172 these biopolymers is higher in the particulate pool, it usually declines to only a few percent in the dissolved pool. TEP is
173 composed of polysaccharides (i.e., CHO) with a major fraction contributing to POC, while a minor fraction exists at the
174 interface between the dissolved and particulate phases (Verdugo et al., 2004). These compounds were selected as they represent
175 major carbon and nitrogen pools in the SML, are widely reported across marine and freshwater systems, and are sufficiently
176 represented in the literature to support a robust meta-analytical assessment.

177 The EF values for these target compounds were systematically calculated from corresponding $[C]_{\text{SML}} - [C]_{\text{ULW}}$ pairs, using Eq.
178 (1). In this study, $[C]_{\text{SML}}$, $[C]_{\text{ULW}}$ and EF data are collectively referred to as ‘primary data’. Auxiliary information associated
179 with the primary data (i.e., sampling factors and environmental variables) was also extracted when reported and is referred to
180 as ‘secondary data’. All analyses were performed using the complete primary data set, independent of whether secondary data
181 were available. The secondary data were summarized only to illustrate existing research gaps in SML studies. All the data
182 were collected either (1) directly from the source when presented, or else (2) through digitization of graphs and plots using
183 PlotDigitizer (<https://plotdigitizer.com>) and GraphClick v3.0 (<https://graphclick.en.softonic.com/mac>). To estimate
184 digitization uncertainty, TOC data (40 datapoints) from Bastrup-Spohr and Staehr (2009) were digitized five times (200
185 values in total). The standard deviation of repeated measurements was calculated for each point and expressed relative to its
186 average. Across all points, the median relative uncertainty was 0.3%, indicating that digitization introduced minimal error. The

187 resulting compiled database is herein referred to as ‘Surface Microlayer Organic Matter Global Data Collection’ (SML-OM).
188 Table S1 provides an overview of the reference studies on which the SML-OM is based.

189 **2.2 Statistical analyses**

190 Given that the SML-OM ranges over several orders of magnitude, when the dataset is handled in linear-space (i.e. in its original
191 form), higher values dominate and overshadow the features associated with lower values (Feenstra, 2006). These potential
192 limitations of linear scaling were reduced by transforming our primary data into their logarithmic (\log_{10}) counterparts.
193 Hereafter, the term ‘linear’ refers to the original, untransformed data, while the term ‘log’ stands for their logarithmic
194 equivalents. The following sections describe the subsequent analyses conducted in our work.

195 **2.2.1 Probability distributions**

196 Making inferences based on ratios such as EF values requires careful consideration, as changes in the numerator and the
197 denominator often affect these ratios asymmetrically (Keene, 1995). In the context of this study, while reductions in $[C]_{ULW}$
198 can lead to unusually high EF values that can approach infinity (i.e., stretched towards higher values), increases in $[C]_{ULW}$ may
199 produce EFs decreasing down to 0 (i.e., compressed towards lower values). This results in distributions that significantly
200 deviate from Gaussian (i.e. normally distributed) shape. Therefore, distributional characteristics of the primary data were
201 examined through probability distributions.

202 Probability density functions (hereafter referred to as ‘PDF’) of the EF values were examined by applying non-parametric
203 Kernel Density Estimates (hereafter referred to as ‘KDE’; Parzen, 1962; Silverman, 2018; Wegman, 1972). KDE employs a
204 normalized weighting function – known as ‘Gaussian kernel’ – which is centered at each datapoint. The sum of these kernels
205 produces a smooth and continuous PDF that fits the underlying data. Selection of the width of a kernel – known as ‘bandwidth’
206 – is an integral part of the KDE approach, as bandwidths too small or too large lead to overfitting and underfitting of data,
207 respectively, failing to capture the true patterns in distributions. Following this, optimal bandwidths for linear KDEs were
208 computed based on Härdle et al. (2004). For log KDEs, a fixed bandwidth was applied. Log transformations, unlike the linear
209 scale, produce similar distributions with comparable spreads across variables, allowing a single fixed bandwidth to produce
210 stable and consistent smoothing for all data.

211 Robustness of the KDE method decreases at low sample size. Since the SML-OM contains variables with sample sizes as low
212 as 16 (for proteins), a bootstrap resampling approach was adopted where 67% of the original data (i.e., $2/3$ of the sample) were
213 randomly subsampled. This proportion balances the need for sufficient data to generate stable KDEs while still introducing
214 variability for robustness testing. By allowing consistent treatment across all data types, this approach maintains comparable
215 KDE bandwidth behavior among subsamples. An individual KDE was generated at each iteration. The process was repeated
216 1000 times, each time with a different random subsample, generating a set of KDE. These were then averaged to produce an

217 ensemble mean, from which the final PDFs were derived. Additionally, cumulative distribution functions (hereafter referred
218 to as ‘CDF’) were determined for $[C]_{\text{SML}}$ and $[C]_{\text{ULW}}$ from the ensemble means of the bootstrapped KDEs. Appendix A provides
219 further information on the KDE method.

220 **2.2.2 Summarization, comparison and correlation estimates of distributions**

221 For describing, comparing and relating the resulting PDFs and CDFs, we used standard statistical measures. Their
222 mathematical expressions are given in Appendix B.

- 223 (1) To describe the central tendencies, mode (hereafter referred to as ‘ x_m ’), median (hereafter referred to as ‘ \tilde{x} ’),
224 arithmetic mean (hereafter referred to as ‘ \bar{x}_a ’) and geometric mean (hereafter referred to as ‘ \bar{x}_g ’), were computed.
- 225 (2) The values at 5th and 95th percentiles of each distribution (hereafter referred to as ‘upper threshold: UT’ and ‘lower
226 threshold: LT’, respectively) were also estimated in order to determine their central 90% range (i.e., degree of spread).
- 227 (3) To numerically compare the $[C]_{\text{SML}}$ and $[C]_{\text{ULW}}$, Integrated Quadratic Distance (Hereafter known as ‘IQD’) values of
228 their CDFs were approximated based on Eq. (B3), which measure how different the two distributions are with regard
229 to symmetry and multimodality.
- 230 (4) To investigate and quantify potential relationships between $[C]_{\text{SML}}$ and $[C]_{\text{ULW}}$ of each target compound, their linear
231 correlation was analyzed by employing both parametric Pearson and non-parametric Spearman’s tests (both methods
232 were applied for cross-validation purposes; agreement between the two correlation coefficient values increases the
233 confidence in the robustness of the observed relationship).

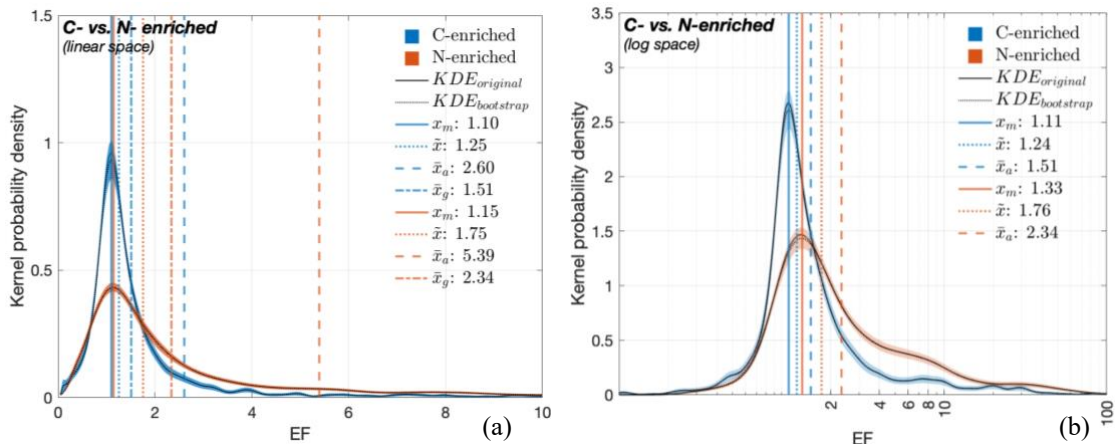
234 **3 Results**

235 Unless otherwise stated, all analyses were performed on log scale. Nevertheless, to avoid potential misinterpretation of log
236 scales in data presentation, primarily due to their limited readability among non-expert audiences (e.g., Menge et al., 2018),
237 all results are presented on linear scale.

238 **3.1 Characterizing EF distributions**

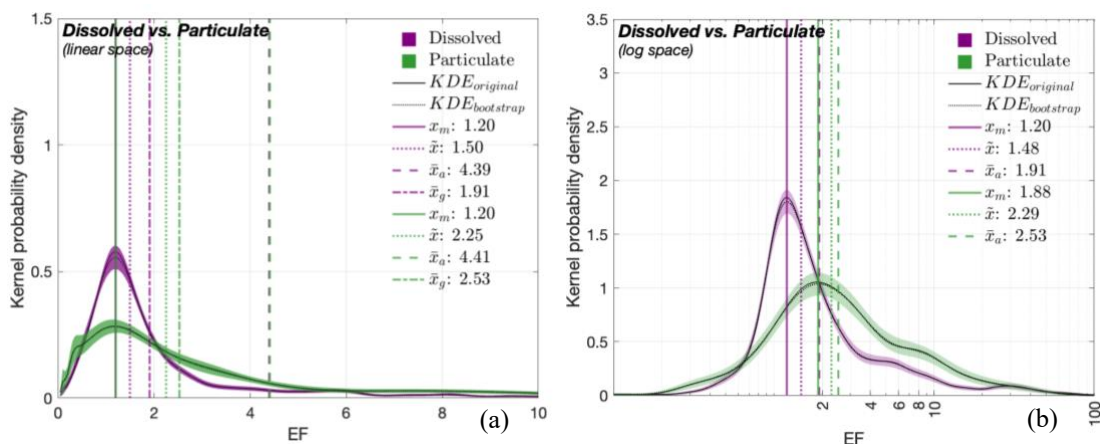
239 Figure 1 compares the KDE-derived PDFs of the EF values for the carbon-enriched (in blue) and nitrogen-enriched (in orange)
240 organic compounds (Hereafter known as ‘PDF_C’ and ‘PDF_N’, respectively). PDF_C was derived from EF values for TOC, DOC,
241 POC, FA, TEP and CHO. The remaining target compounds derive PDF_N. In their linear version (Figure 1(a)), both PDFs
242 demonstrate positive skewness (i.e., right-skewness) with the two x_m values being 1.10 and 1.15, respectively. Nevertheless,
243 the peak probability density of the PDF_C (i.e., the height of the PDF = ~1) is more than twice that of the PDF_N (~0.4). \tilde{x} of the
244 two PDFs vary substantially, with PDF_C and PDF_N yielding values of 1.25 and 1.75, respectively. The values for \bar{x}_a (2.60 and
245 5.39, respectively) and \bar{x}_g (1.51 and 2.34, respectively) further reflect this divergence. In contrast, their log-transformed

246 versions (Fig. 1(b)) approximate normal distributions, with PDF_C estimating the (exponentials of) $x_m = 1.11$; $\bar{x} = 1.24$ and \bar{x}_a
 247 = 1.51. The PDF_N yields corresponding values of 1.33, 1.76 and 2.34. Their peak probability densities also reflect that the
 248 PDF_C (~ 2.6) is twice as high as that of PDF_N (~ 1.5).



249 **Figure 1: PDFs of the EF values for carbon-enriched (blue) and nitrogen-enriched (orange) compounds.** PDFs of the (a) untransformed
 250 (i.e., linear) and (b) log-transformed EF values. The solid black line indicates the KDEs derived from original data while the dashed black
 251 line represents the ensemble mean of bootstrapped KDEs. Central tendency metrics (mode [x_m], median [\bar{x}], arithmetic mean [\bar{x}_a], geometric
 252 mean [\bar{x}_g]) given in panel (b) are the exponentials of the corresponding estimates on the log scale.

253 We also compared EF-based PDFs (Figure 2) for dissolved (PDF_D , in purple) and particulate (PDF_P , in green) OM where we
 254 refer to a filter size of $0.22 \mu\text{m}$ (Gao et al., 2012). At a linear scale (Figure 2(a)), the PDFs are again right-skewed for the two
 255 clusters, with characteristics: (1) 1.20 (both PDF_D and PDF_P) for x_m ; (2) 1.50 and 2.25 for \bar{x} ; (3) 4.39 and 4.41 for \bar{x}_a and, (4)
 256 1.91 and 2.53 for \bar{x}_g , respectively. The peak probability density of the PDF_D (~ 0.6) exceeds that of the PDF_P (~ 0.3) by nearly
 257 a factor of two. The log PDF_D and PDF_P (Fig. 2(b)) approximate normal distributions alongside the following exponentiated
 258 central values, respectively: (1) $x_m = 1.20$ and 1.88; (2) $\bar{x} = 1.48$ and 2.29; (3) $\bar{x}_a = 1.91$ and 2.53. Their peak probabilities
 259 compare between ~ 1.8 (for PDF_D) and ~ 1.0 (for PDF_P).

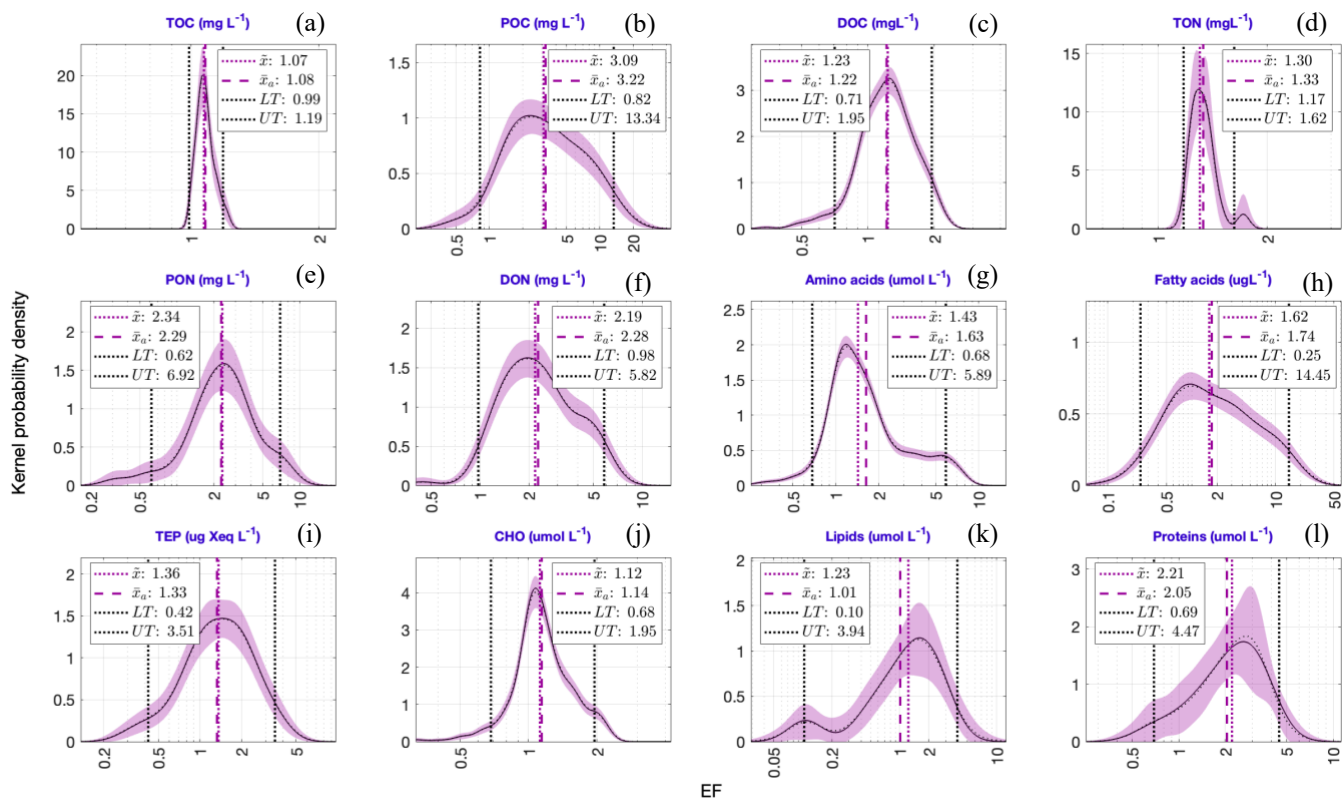


260 **Figure 2: PDFs of the EF values for dissolved (purple) and particulate (green) compounds.** PDFs of (a) linear and (b) log EF values.
 261 See Fig. 1 caption for details on KDEs and central tendency metrics.

262 Figure 3 displays the PDFs of the EF values for the target compounds. All the distributions exhibit nearly log-normal
 263 characteristics, nevertheless they vary in their degrees of spread. Here, only \tilde{x} and \bar{x}_a values estimate the central tendency of
 264 each distribution (the rationale for this approach is discussed in section 4.2). The values of \tilde{x} (dotted pink line) and \bar{x}_a (dashed
 265 pink line) are closely aligned in magnitude. According to these derived estimates, median and geometric mean EFs are largest
 266 for POC (Fig. 3(b): $\tilde{x} = 3.09$; $\bar{x}_a = 3.22$) across all the target compounds, with PON (Fig. 3(e)) and DON (Fig. 3(f)) following
 267 closely, each exhibiting \tilde{x} and \bar{x}_a values > 2 . Although proteins (Fig. 3(l)) also show higher central tendency estimates, it
 268 should be noted that they have the smallest sample size (= 16), followed by lipids (sample size = 20). Therefore, the results of
 269 these two compounds should be interpreted with caution due to their lower statistical robustness. A comparison of threshold
 270 metrics (i.e., LT and UT; see section 2.2.2) reveals that the EF distributions for FA (Fig. 3(h)) and POC (Fig. 3(b)) exhibit the
 271 highest UT values (14.5 and 13.3, respectively) along with the greatest distributional variability. TOC (Fig. 3(a)) and TON
 272 (Fig. 3(d)) show the least variability among all target compounds. While some compounds exhibit well-defined unimodal EF
 273 distributions (e.g., POC, PON), few others (e.g., TON, AA) display polymodal patterns.

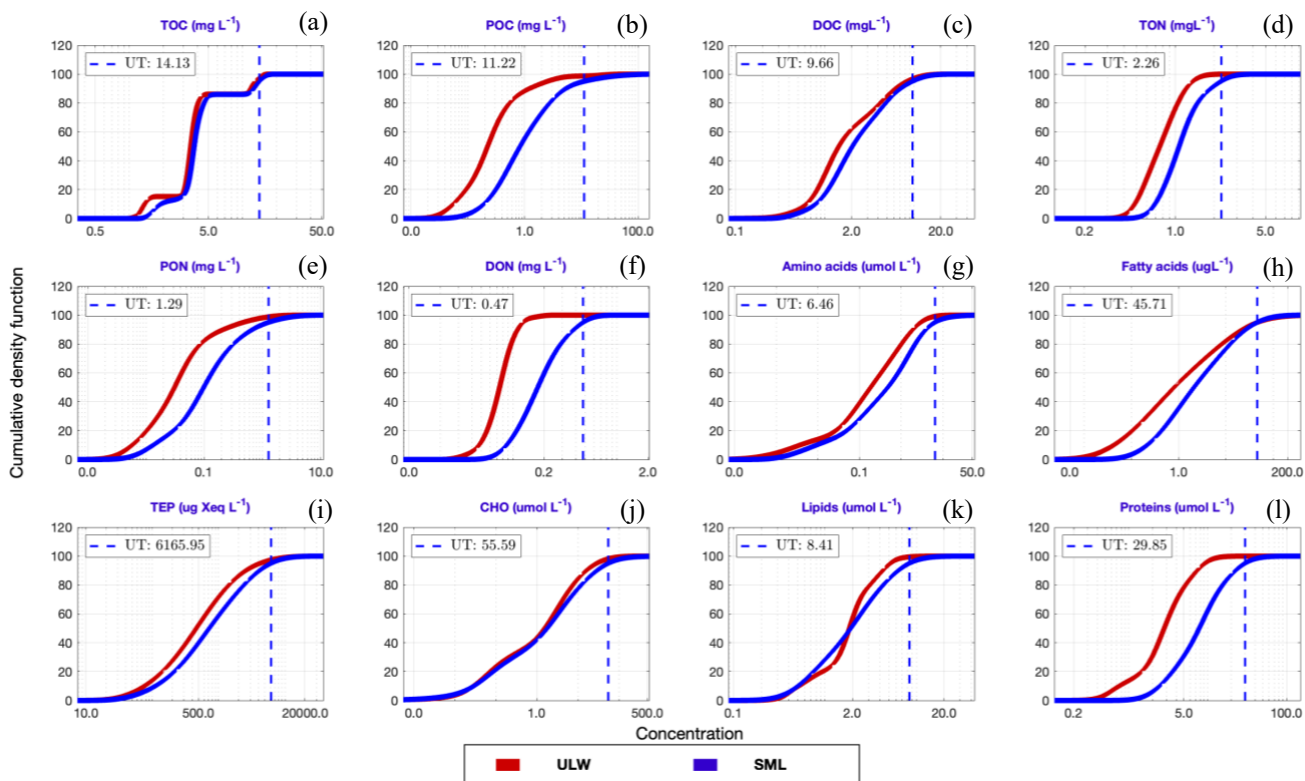
274 3.2 Comparing SML and ULW concentrations

275 Figure 4 presents the CDFs of the ULW (in red) and SML (in blue) concentrations for the target compounds. A CDF exhibits
 276 how probability accumulates across a range of values (in the current context, $[C]_{\text{SML}}$ and $[C]_{\text{ULW}}$ data). All CDFs (both $[C]_{\text{ULW}}$
 277 and $[C]_{\text{SML}}$) exhibit a characteristic sigmoidal shape: a slow initial rise (i.e., lag phase), followed by a steep rise (i.e.,
 278 exponential phase), eventually reaching a plateau (i.e., stationary phase). CDFs for TOC display two distinctive plateaus
 279 indicating bimodal concentration distributions for both SML and ULW.



280 **Figure 3: PDFs of the EF values for the twelve target compounds.** The lower and upper thresholds of each distribution (dashed black
 281 lines) are defined by 5th and 95th percentiles of each PDF (see section 2.2.2). The values of these thresholds, along with the central tendency
 282 metrics given in each panel, are the exponentials of the corresponding estimates in the log space.

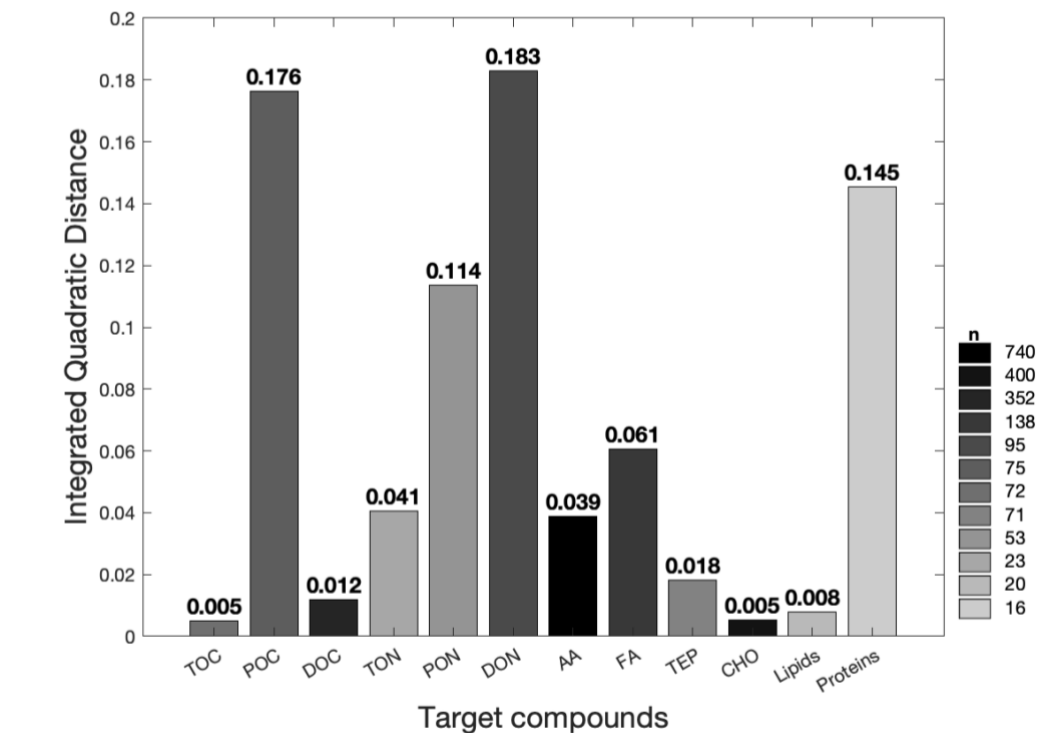
283 Additionally, despite the homogeneity in the general shape and trend of these CDFs, their corresponding IQDs (Fig. 5) reveal
 284 that the magnitudes of the offsets between $[C]_{ULW}$ and $[C]_{SML}$ distributions vary substantially across the target compounds.
 285 Lower IQD values indicate greater similarities between the CDFs, while higher values document clear distinguishability and
 286 thus also document a more robust enrichment signal. The lowest IQD is reported for the CDFs of TOC and CHO (0.005) while
 287 that of DON yields the highest in value (0.184). In addition, lower CDFs (i.e. IQD < 0.05) are observed for lipids (0.008),
 288 DOC (0.012), TEP (0.018), AA (0.039) and TON (0.041), whereas POC (0.18) and proteins (0.15) exhibit a greater divergence
 289 (i.e. IQD > 0.15) between $[C]_{ULW}$ and $[C]_{SML}$. The color intensity of each bar reflects the sample size (n) of each target
 290 compound (i.e., smaller the sample, lighter the color).



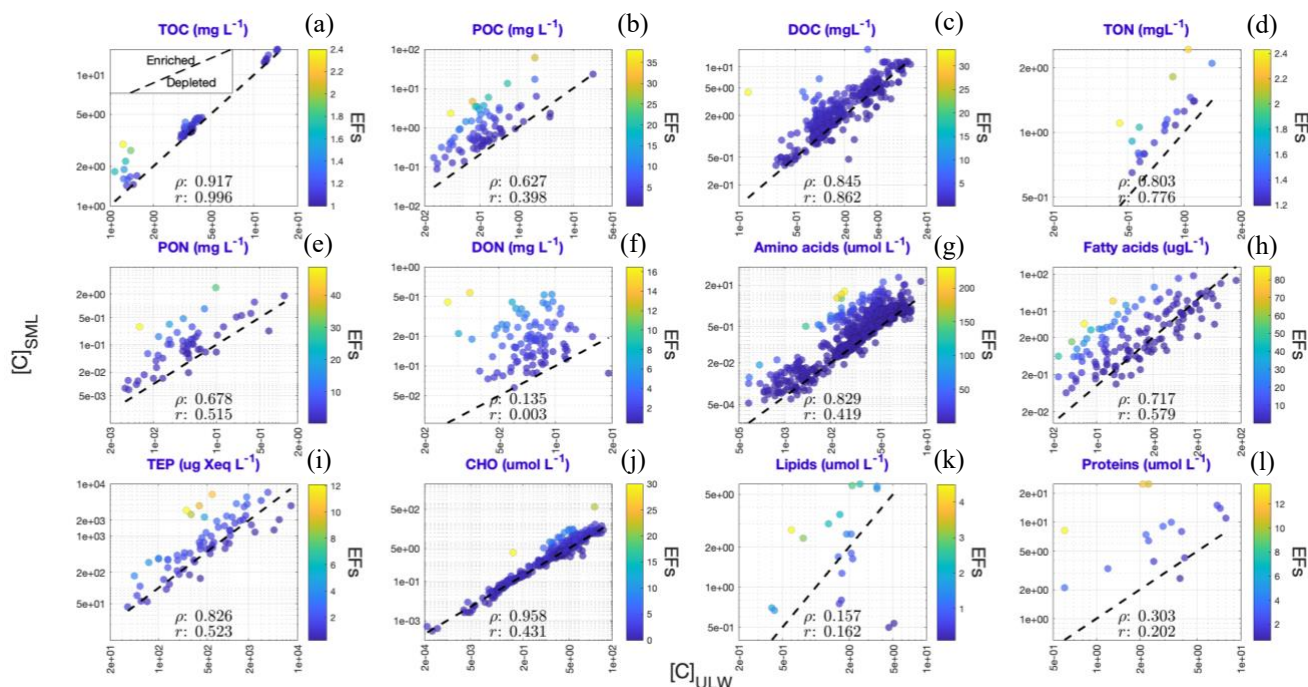
291 **Figure 4: CDFs of the ULW (red) and SML (blue) concentrations for the target compounds.** The upper thresholds for $[C]_{\text{SML}}$ (UT; 292 given by blue dashed lines) are defined by 95th percentiles of the corresponding CDF. The values of these thresholds are the exponentials of 293 the corresponding estimates in the log space. Their corresponding IQDs are given in Figure 5.

294 Correlations between $[C]_{\text{ULW}}$ and $[C]_{\text{SML}}$ of the target compounds were statistically estimated using liner correlation, as 295 presented in Figure 6. The coefficients ‘ ρ ’ and ‘ r ’ stand for the correlation values derived from non-parametric Spearman’s 296 and parametric Pearson correlation tests, respectively. For all target compounds, except for DON, lipids and proteins, we found 297 strong correlations between their SML and ULW concentrations (ρ and $r > 0.5$) with robust positive relationships. Individual 298 datapoints for TOC, DOC and CHO (Figs. 6(a), (c) and (j)) closely fall on the 1:1 reference line where $[C]_{\text{SML}} = [C]_{\text{ULW}}$ (dashed 299 black line). In contrast, those for POC, TON, AA and FA are notably shifted towards the y-axis, suggesting higher $[C]_{\text{SML}}$ 300 values relative to $[C]_{\text{ULW}}$ that correspond to potentially enriched (depleted) SML (ULW) concentrations against ULW (SML) 301 concentrations (see inset plot in Fig. 6(a)). Although TEP shows a slight enrichment in the SML, the effect is not particularly 302 pronounced (Figure 6(i)). In addition, all the datapoints (regardless of whether they display copulation or not) were further 303 color-coded according to their respective EFs. The results reveal an overall consistency in EFs across concentration ranges

304 irrespective of their magnitudes. For example, in Fig. 6(c), EF values remain below 5, both when $[C]_{ULW}$ and $[C]_{SML}$ are < 0.5
305 mg L^{-1} and $> 5 \text{ mg L}^{-1}$. This pattern holds across nearly all the target compounds.



306 **Figure 5: IQD values quantifying the divergence between ULW and SML concentrations for each target compound.** The IQD
307 represents the squared difference between ULW- and SML-based CDFs shown in Figure 4. Higher IQD indicates greater divergence between
308 the two distributions and vice versa. Bar color intensity corresponds with the sample sizes.



309 **Figure 6: Linear correlation between $[C]_{ULW}$ and $[C]_{SML}$ for the target compounds.** The datapoints are color-coded based on their
 310 corresponding EFs. Dashed black line indicates 1:1 line when $[C]_{ULW}$ (x-axis) = $[C]_{SML}$ (y-axis). Inset plot in panel (a) exhibits the relevant
 311 implications of the figure: Correlations above the 1:1 line corresponds to selective SML enrichment and vice versa. The values of 'ρ' and
 312 'r' give Spearman's and Pearson correlation coefficients, respectively.

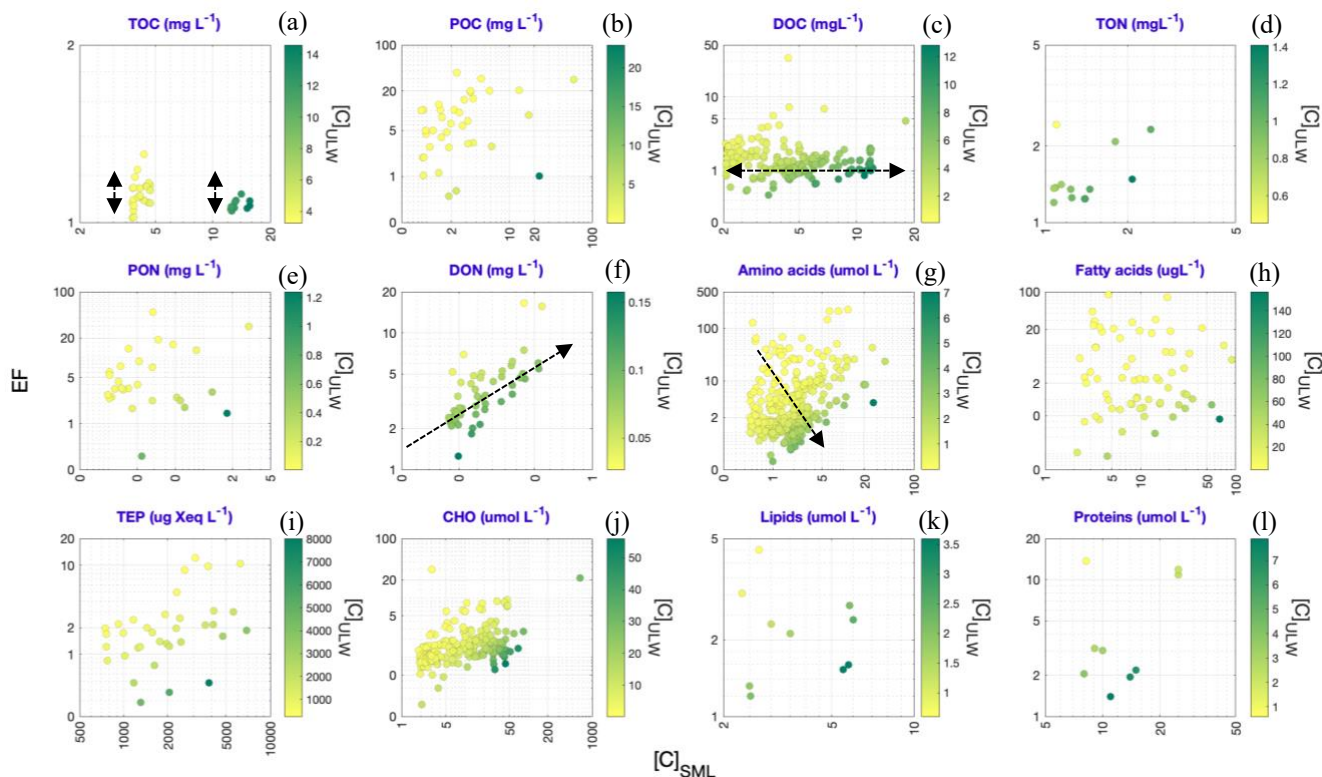
313 3.3 Investigating concentration-dependent enrichment dynamics

314 Informed by the observations drawn from Fig. 6, Fig. 7 presents a more detailed investigation into the interrelationships among
 315 $[C]_{SML}$, $[C]_{ULW}$ and EFs in the environment. The analysis is restricted to $[C]_{SML}$ values (x-axis) that exceed the \tilde{x} (i.e., median)
 316 of their respective distributions (median is the most stable central tendency metric of a distribution. Discussed further in section
 317 4.2). These elevated $[C]_{SML}$ are compared against the corresponding $[C]_{ULW}$ (color scale) and EF (y-axis) values. The results
 318 reveal following covariation trends:

- 319 (i) TOC reports a generally low range of EF values comparable at both low and high concentrations of SML and
 320 ULW (Fig. 7(a))
- 321 (ii) DOC displays relatively consistent EF values regardless the magnitudes of $[C]_{SML}$ and $[C]_{ULW}$ (Fig. 7(c)), but
 322 also slightly points towards higher EF values in association with low $[C]_{ULW}$
- 323 (iii) DON presents an ascending EF gradient, positively correlated with $[C]_{SML}$ (Fig. 7(f)), revealing more enrichment
 324 to be well reflected in the concentrations found in the SML

325 (iv) AA shows a similar correlation dependence to that of DON, but also reveals a much clearer trend toward higher
326 EF values to be found at lower $[C]_{ULW}$ concentrations (Fig. 7(g))

327 FA (Fig. 7(h)), despite their larger sample sizes, exhibit no clear trend in the $[C]_{SML} - [C]_{ULW} - EF$ triad.



328 **Figure 7: Interdependent relationship of $[C]_{SML}$ values with the corresponding $[C]_{ULW}$ and EF values.** The analysis is restricted to
329 $[C]_{SML}$ values that exceed the corresponding \bar{x} values. The x-axes give the observed $[C]_{SML}$ values against their corresponding EF values on
330 y-axes. Datapoints are color-coded based on corresponding $[C]_{ULW}$ values. The black arrows indicate identified enrichment patterns.

331 4. Discussion

332 A major strength of the SML-OM dataset is its broad coverage of OM concentrations, whereas individual studies are typically
333 restricted to a narrow range of similar ULW conditions. By employing a meta-analytical approach, our study presents the first
334 comprehensive overview of the enrichment dynamics in the SML, based on existing literature. Meta-analytical studies offer a
335 rigorous framework to synthesize evidence across diverse datasets thereby improving the reliability of scientific conclusions.
336 By statistically integrating outcomes from independent investigations, meta-analyses increase overall analytical power, reduce
337 the influence of small-sample variability and, uncover true environmental signals from study-specific biases (i.e., sampling

338 strategies, analytical techniques, spatial scales and seasonality). This not only enhances the generalizability of findings but
339 also exposes gaps and inconsistencies in the existing literature, guiding the development of more robust future studies.

340 In this context, conducting a quantitative assessment of how the reference studies (i.e., those on which the SML-OM is based)
341 are distributed across key domains of SML research provides insights into the most frequently studied aspects (Figure S1),
342 thereby explicitly quantifying metadata coverage; research on the SML has increased from about 15 publications per year in
343 the early 2000s to approximately 50 per year by 2016 (Engel et al., 2017). However, our work highlights the potential
344 understudied areas in SML research that call for more in-depth analysis. For instance, majority of the reference studies has
345 been conducted in oceanic and coastal regions (~76% of data) and predominantly during warmer months (~77% of data) with
346 a significant mismatch observed for data collected under low and high wind regimes (~81% vs. 19%, respectively). In light of
347 these research gaps, the following sections interpret the main findings revealed by our analysis and discuss their implications
348 for understanding SML enrichment.

349 **4.1 Overarching trends in SML enrichment**

350 **4.1.1 Generalized enrichment patterns**

351 Comparison of KDE-derived PDFs for the EF values of (1) carbon-enriched vs. nitrogen-enriched organic compounds (Fig. 1)
352 and (2) dissolved vs. particulate organic compounds (Fig. 2) yield the following key implications:

- 353 (1) All the estimated original (i.e., linear scale) PDFs (Figs. 1(a) and 2(a)) display higher probability densities for lower
354 EF values and extended tails towards higher EF values (i.e., right-skewness), suggesting that under natural conditions,
355 modest SML enrichment is far more common in general, while extreme enrichment events are rare
- 356 (2) Variations in the peak probability densities among the PDFs indicate that extreme SML enrichment events are
357 relatively more frequent in nitrogen-enriched compounds (Fig. 1: orange PDF) and particulate forms (Fig. 2: green
358 PDF), compared to carbon-enriched compounds (Fig. 1: blue PDF) and dissolved forms (Fig. 2: purple PDF)
- 359 (3) Nitrogen-enriched compounds and particulate forms exhibit a broader EF variability (i.e., higher mode, median, mean
360 values) compared to carbon-enriched compounds and dissolved forms with a relatively more consistent spread (i.e.,
361 lower central tendency metrics)

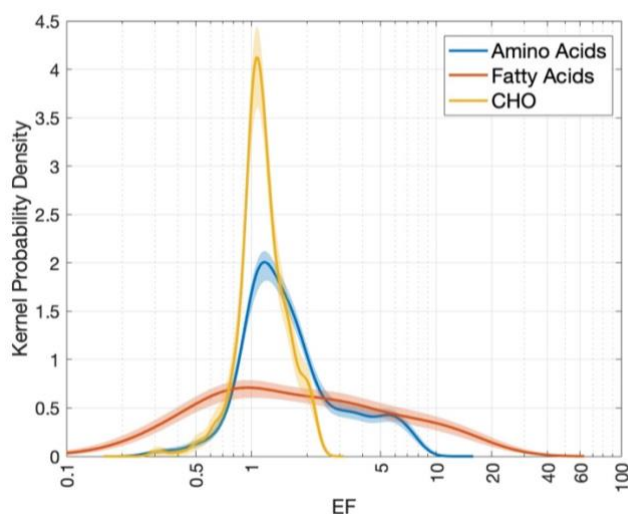
362 These differences in peaks and central tendency metrics persist in log-transformed PDFs as well (Figs. 1(b) and 2(b)). This
363 validates that these variations are not caused by statistical artifacts but reflect real, natural variability in enrichment behavior.
364 Overall, these findings from our meta-analysis indicate that the OM accumulation in the SML is more effective for (1) nitrogen-
365 enriched than for carbon-enriched compounds and (2) particulate than for dissolved forms. These enrichment patterns likely
366 reflect the combined influence of biological, chemical and physical mechanisms acting on the SML: Frka et al. (2012) outlined

367 the complex, multicomponent behaviour of the SML, suggesting competitive adsorption of more insoluble surfactants (e.g.,
368 lipid-like material) during highly productive seasons. Selective enrichment of certain polar amino acids (e.g., arginine and
369 glutamic acid) relative to others has been hypothesized (Barthelmeß and Engel, 2022). However, these mechanisms are not
370 yet fully resolved. The molecular structure of N-enriched compounds also promotes aggregation into colloids or microgel
371 particles (Dietz et al., 1976), a process further enhanced by bubble scavenging and low-turbulence trapping (Mopper et al.,
372 1995). In contrast, carbon-rich compounds such as polysaccharides are generally more soluble and tend to remain largely
373 distributed in the bulk water, resulting in comparatively lower surface activity and enrichment at the interface (Ćosović and
374 Vojvodić, 1989; Laß et al., 2013). Similarly, particulate OM exists as discrete, larger units, that can be trapped at the interface
375 due to surface tension and by bubble-mediated processes (Robinson et al., 2019). However, some particles, such as TEP
376 ballasted with mineral dust or phytoplankton shells, may sink rather than rise, highlighting the complex balance of forces
377 controlling surface accumulation (Mari et al., 2017). While bubble scavenging represents a process which can lead to the
378 aggregation of dissolved components (for example, at the rear of rising bubbles; Dukhin et al., 2015; Zhou et al., 1998), a large
379 fraction of dissolved OM, potentially exhibiting reduced overall surface activity, passes through these processes without
380 accumulating at the air–water interface. Transient enrichment of dissolved OM can nonetheless occur. Overall, surface-
381 associated processes such as bubble scavenging and aggregation can enhance the enrichment of particulate compounds in the
382 SML relative to dissolved forms.

383 Our findings contradict some earlier works, including (Baastrup-Spohr and Staehr, 2009; Liss and Duce, 1997; Yang, 1999),
384 who suggest that the SML is similarly enriched for both particulate and dissolved organic (and inorganic) compounds, but
385 align with other studies that report opposing results: Dietz et al. (1976) provide evidence for enhanced accumulations of
386 particulate matter in the SML through particle aggregation at the surface. The work further links high abundances of living
387 bacteria in the near-surface to higher availability of POC in the SML. Studies of Carlucci et al. (1985), Henrichs and Williams,
388 (1985), Kuznetsova et al. (2004), Kuznetsova and Lee (2002) and Reinthaler et al. (2008) report that POC and PON tend to be
389 more enriched in the SML than DOC. Engel et al. (2017) state that the SML has been shown to be enriched in particulate
390 organic matter, particularly in proteinaceous compounds. Together, these findings and our meta-analytical synthesis, indicate
391 that nitrogen-enriched compounds may interfere more critically with interfacial properties. Whether incorporating these
392 nitrogen-based metrics can improve the precision of traditional carbon-only parameterizations of gas exchange suppression
393 (e.g., Barthelmeß et al., 2021; Li et al., 2024) remains an important question for future work.

394 Although nitrogen-enriched compounds seem to exert a strong influence on the SML's interfacial properties at the bulk scale,
395 a compound-specific comparison of three biosurfactants data – AA (Fig. 3(g)), FA (Fig. 3(h)) and CHO (Fig. 3(j)) – reveals a
396 more complex picture (Figure 8): AA, despite their high nitrogen content, do not exhibit the highest enrichment. Instead, their
397 EF values (0.3 – 10) fall between those of CHO (lower end: 0.3 – 2.5) and FA (upper end: 0.1 - 60). Our results are consistent
398 with earlier reports on their natural EF ranges: Polysaccharides can be enriched in the SML up to three-fold compared to the

399 ULW (Williams et al., 1986; Wurl and Holmes, 2008). Enrichment of AA can vary between 0.3 to 201, depending on their
400 species-specificity (Cunliffe et al., 2013). This EF hierarchy likely reflects the intermediate surface activity of these three
401 compounds: Barthelmeß and Engel (2022), referring to Ćosović and Vojvodić (1998) state that “*Lipid-like surfactants exhibit*
402 *stronger surface activity, while protein-like, followed by carbohydrate-like, surfactants decrease in activity*”. FA dominate
403 competitive adsorption due to their strong amphiphilic character (i.e., a long hydrophobic tail and small polar head), allowing
404 them to readily form stable monolayers at the interface. In contrast, proteins are moderately surface-active, while highly soluble
405 CHO largely remain in the bulk water (Ćosović and Vojvodić, 1998; Laß et al., 2013; Laß and Friedrichs, 2011). Consequently,
406 these patterns suggest that compound-specific enrichment in the SML is driven more by the surfactant properties of individual
407 compounds than their elemental composition alone. While this hierarchy holds for single-component systems, interactions in
408 natural SML mixtures are complex, and the structural properties of the nanolayer are influenced by both rare insoluble lipid-
409 like and abundant soluble carbohydrate-like material. Nevertheless, we do not extend this analysis further as biosurfactant
410 measurements (1) primarily quantify surface activity rather than enrichment and (2) are subjected to methodological
411 inconsistencies that limit cross-study comparability. We further acknowledge that the mechanistic links between surfactants,
412 their behavior and associated ecosystem processes remain incompletely understood.



413 **Figure 8: Comparison of PDFs of the EF values for three biosurfactants: Amino acids (blue), fatty acids (orange) and carbohydrates**
414 (yellow). The figure synthesizes the KDEs given in Figs. 3(g), (h) and (j).

415 Overall, these overarching trends of SML enrichment underscore the importance of resolving compound-specific accumulation
416 in the SML, while distinguishing between selective and non-selective enrichment. Cumulative probability comparison results
417 for the $[C]_{ULW}$ and $[C]_{SML}$ (Figs. 4 and 5) and their corresponding linear correlations (Fig. 6) provide a meta-analytical

418 perspective on how compounds are distributed and accumulated between the two compartments. Here, results concerning
419 lipids and proteins are excluded due to apparent randomness in their distributions, potentially caused by smaller sample sizes.

420 **4.1.2 Compound-specific enrichment patterns**

421 Significant correlations between $[C]_{ULW}$ and $[C]_{SML}$ of nearly all the target compounds (ρ and $r > 0.5$) are consistent with the
422 overall understanding that the SML's composition is linked to the availability of material in the underlying sub-surface waters
423 (Chen et al., 2016; Joux et al., 2006). Contrary to this general pattern, (Kuznetsova et al., 2004) suggest that certain OM
424 fractions in the SML and ULW may show lack of correlation, potentially due to constraints such as varying mineralization
425 rates between the two layers and surface adsorption processes. Consistent with this view, linear correlation results for DON
426 indicate such decoupling (Fig. 6(f)), though the underlying causes remain unexplored in this study. Early works also suggested
427 that the variations in the SML concentrations are typically larger than those in the ULW (Reinthal et al., 2008). In agreement,
428 CDFs of the $[C]_{ULW}$ and $[C]_{SML}$ demonstrate faster probability accumulation for ULW than SML (Fig. 4), implying generally
429 smaller magnitudes and lower variability in ULW concentrations compared to SML concentrations. Conversely, Carlson
430 (1983) argues that, in certain occasions, OM variability in the SML and ULW may not significantly differ across temporal and
431 spatial scales. The CDFs for TOC, DOC, TEP and CHO which exhibit the lowest IQD values (Fig. 5) support this but is
432 contradicted by those of the other compounds, with higher IQD values (indicating substantial differences between the two
433 concentrations).

434 Works of Hunter and Liss (1977) and Kurata et al. (2016) discuss the selective enrichment of surfactants in the SML, mainly
435 driven by microbial processes. Hydrophobic compounds tend to show more affinity to the surface compared to hydrophilic
436 substances (Marty and Saliot, 1976). In agreement, our linear correlation results reveal preferential accumulation of the
437 biosurfactants, AA (Fig. 6(g)) and FA (Fig. 6(h)), in the SML. Linear correlation results shown in Fig. 6(i) provide evidence
438 to the view that TEP is generally enriched in the SML compared to the ULW (Cunliffe et al., 2009; Cunliffe and Murrell,
439 2009; Wurl and Holmes, 2008), although this enrichment is not strongly pronounced in our dataset. Additionally, the nearly
440 overlapping CDFs for TEP in SML and ULW (Fig. 4(i)) along with its low IQD value ($= 0.081$; Fig. 5) indicate a surprisingly
441 weak enrichment, contrary to expectations. Nevertheless, concentration trend of TEP observed in our data closely aligns with
442 that of CHO (Figs. 4(j) and 5), supporting the prevailing hypothesis that TEP is formed through coagulation of dissolved
443 polysaccharides (Passow, 2000). Thornton et al. (2016) observe that TEP and dissolved polysaccharides do not always exhibit
444 significant enrichment in the SML as anticipated.

445 POC and PON correlation patterns (Figs. 6(b) and 6(e), respectively) where $[C]_{SML}$ significantly exceeds $[C]_{ULW}$, and that of
446 DOC (Fig. 6(c)) where $[C]_{SML}$ is nearly equal to $[C]_{ULW}$, provide strong meta-analytical evidence to earlier works that discuss
447 the selective enrichment of POC and PON in the SML over DOC (e.g., Henrichs and Williams, 1985; Kuznetsova et al., 2004;
448 Kuznetsova and Lee, 2002; Reinthal et al., 2008). Carlson (1983) suggests that the distribution of some organic fractions

449 between the SML and the ULW may be governed by specific partitioning processes. For instance, while Chen et al. (2016)
450 point out the significant role of the ULW in DOC and CHO accumulation in the SML, Dietz et al. (1976) observe fairly
451 consistent abundances for these compounds between the two layers. Our experiments also show strong 1:1 correlation for DOC
452 (Fig. 6(c)) and CHO (Fig. 6(j)), suggesting an absence of preferential affinity towards the SML (unlike surfactants), which
453 further indicates that their enrichment is predominantly controlled by the ULW. Although CHO, AA and FA are identified to
454 be the key constituents of the organic carbon pool (Hedges et al., 1994), our correlation results reveal that their partitioning
455 between the SML and the ULW and, their eventual enrichment patterns, may not be consistent (Figure 6), as also suggested
456 by Fig. 8.

457 **4.1.3 Influencing factors and current uncertainties**

458 Baier et al. (1974), Hunter and Liss (1981) and MacIntyre (1974) argue that the compositional diversity of the SML prevents
459 single compounds from fully representing the dissolved OM class, which further emphasizes the importance of assessing
460 compound-specific accumulation in the SML. Such investigations could shed light on selective and non-selective enrichment
461 dynamics of OM. An analysis of EF-based PDFs for various AA fractions (Figure 9(a)) – Total AA (TAA), Dissolved Free
462 AA (DFAA), Dissolved Combined AA (DCAA) and Particulate AA (PAA) – revealed notable heterogeneity within this
463 compound class, reflecting the chemical diversity and complexity of OM enrichment in the SML: Relatively lower enrichment
464 in DFAA may indicate its limited accumulation in the SML, potentially due to its high solubility and rapid turnover (Jørgensen
465 et al., 1993). In contrast, DCAA, which comprises combined amino acids, might exhibit stronger surface activity and a greater
466 tendency to form aggregates, leading to higher enrichment across a broader range. The bimodal EF distribution observed for
467 PAA could reflect differences in particle composition, size and hydrophobicity, whereby denser particles sink rapidly while
468 buoyant, organic-rich particles preferentially accumulate at the surface. TAA, which integrates all these molecular states, may
469 dampen these extremes and yields more moderate enrichment. These interpretations remain as hypotheses, as very little is
470 known about the behavior of AA embedded in highly complex structures in natural SML.

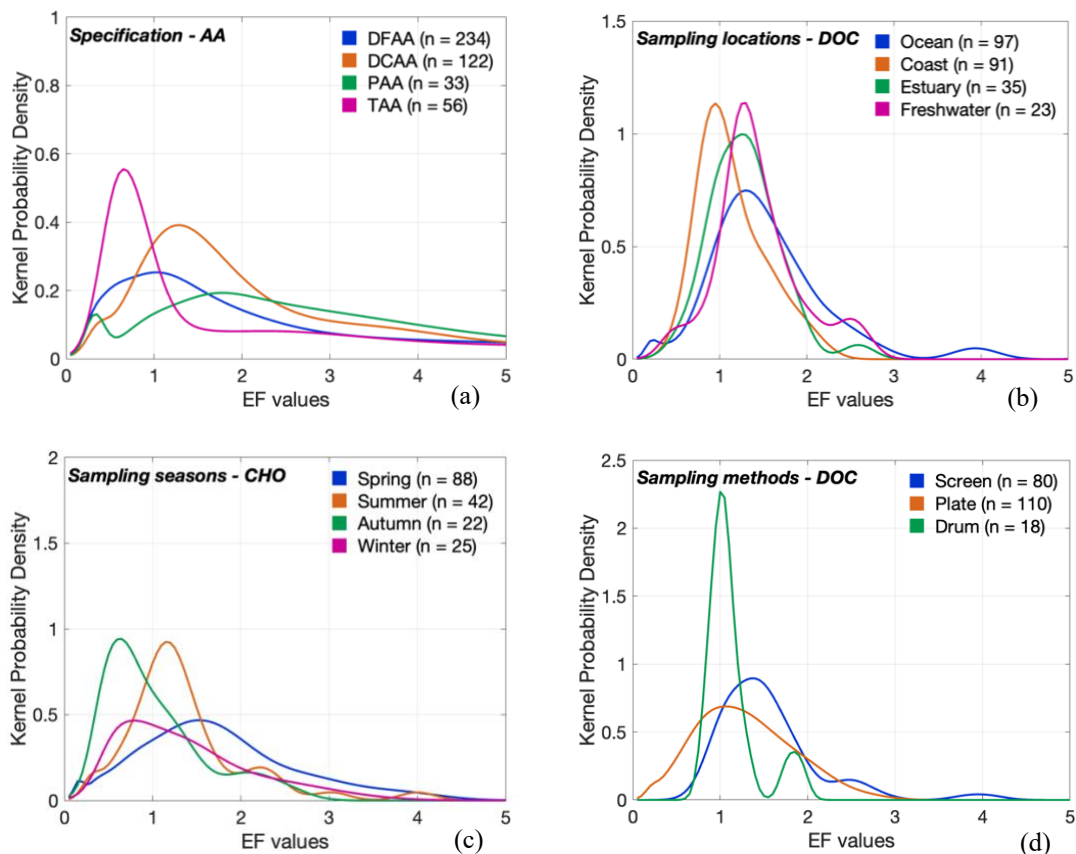
471 Additionally, consistent with previous studies that investigated the influence on environmental drivers on the enrichment
472 dynamics in the SML (e.g., Asher, 1997; Barthelmeß et al., 2021; Knulst et al., 1997; Kuznetsova et al., 2004; Liu and Dickhut,
473 1998; Obermosterer et al., 2008; Reinthaler et al., 2008; Tsai and Liu, 2003), our analysis demonstrates that factors such as
474 sampling location (for DOC), sampling season (for CHO) and sampling method (for DOC) (Figs. 9(b) – (d)) play key roles in
475 modulating the enrichment variability of the OM. It should be noted that these specific target compounds are chosen as
476 representative examples because they span all subcategories of secondary data considered in the study (see Table S1), and
477 therefore enable a more robust comparison among different settings.

478 Comparison of DOC enrichment across four sampling locations (Fig. 9(b)) reveals relatively reduced coastal enrichment (as
479 also seen by Carlson, 1983). This pattern may result from enhanced mixing and shorter surface residence times due to stronger

480 wave action, tidal influence, or nearshore turbulence. Alternatively, the limited two-dimensional space at the air-sea interface
481 in combination with a highly saturated underlying water layer could also contribute to reduced enrichment. At the same time,
482 broader EF variability displayed by oceanic sites likely stems from the greater heterogeneity of open-ocean conditions
483 including varying biological productivity and OM sources (Carlson, 1983). In contrast, estuarine and freshwater systems,
484 which often have more constrained physical regimes and relatively consistent OM inputs, tend to exhibit narrower EF ranges
485 (Hillbricht-Ilkowska and Kostrzewska-Szlakowska, 2004). Observations by Barthelmeß et al. (2021) and Mustaffa et al. (2018)
486 suggest that changes in EF in these systems are driven more by variations in the ULW than by the SML itself, consistent with
487 the idea that the surface layer in high-OM regimes is already saturated and thus less responsive to additional inputs. Moreover,
488 bimodal CDFs of TOC for the SML and ULW concentrations (Fig. 4(a)) along with the distinct separation of three data clusters
489 in their correlation patterns (Fig. 6(a)), further highlight the significant role of spatial factors in shaping SML composition.
490 The origins of TOC data used in this study illustrate this variability: Data from (1) a heavily polluted urban lake (concentration
491 range: 12 – 16 mg L⁻¹; Bastrup-Spohr and Staehr, 2009), (2) a forested lake (concentration range: 3 – 5 mg L⁻¹; Bastrup-
492 Spohr and Staehr, 2009), (3) the Arctic Ocean (concentration range: 1 – 3 mg L⁻¹; Gao et al., 2012) and (4) an upwelling
493 filament (concentration range: 3 – 4 mg L⁻¹; Barthelmeß et al., 2021).

494 Seasonal comparison of the EF values for CHO (Fig. 9(c)) likely reflects temporal differences in biological drivers (Gašparović
495 and Čosović, 2001; 2003) in the SML (i.e., depletion in cold months, while warm months show relatively higher and consistent
496 enrichment with broader variability). Additionally, stronger wind conditions typical of winter may disturb the SML and reduce
497 particle residence time, counteracting surface accumulation (Sun et al., 2018). However, the influence on wind speed on SML
498 enrichment remains ambiguous; our comparison of EF values under calm (< 6.6 ms⁻¹; Reinthaler et al., 2008) and rough (> 6.6
499 ms⁻¹) wind conditions yield inconclusive results (Figure S2) with wind speed appearing to have little/no effect on the SML
500 enrichment (e.g., Bastrup-Spohr and Staehr, 2009; Sabbaghzadeh et al., 2017) or with enrichment persisting even under rough
501 sea conditions (e.g., Kuznetsova et al., 2004; Reinthaler et al., 2008), opposing the general understanding that turbulent
502 conditions may reduce the concentration in the SML (e.g., Carlson, 1983).

503 Nevertheless, it is important to note that imbalanced sampling efforts among these categories (Figure S1), especially with
504 regards to wind speed (Figure S2; see the sample sizes), may compromise the robustness and validity of these findings. This
505 is also evident in the comparison of sampling techniques for the EF values of DOC (Fig. 9(d)), where the drum method, with
506 a sample size of only 17, shows limited variability compared to the screen and plate methods (sample sizes of 80 and 110,
507 respectively). This likely reflects a bias due to sampling effort rather than a true difference in enrichment behavior.
508 Collectively, these findings highlight the need for future SML research and SML-based model development to systematically
509 account for wind and sea-state conditions, and to explore how enrichment patterns may vary under different environmental
510 regimes and methodological settings.



511 **Figure 9: Factor-specific enrichment variability in the SML.** PDFs illustrating varying enrichment patterns for (a) AA across chemical
 512 forms, (b) DOC across sampling locations, (c) CHO across sampling seasons and (d) DOC across sampling methods. ‘n’ gives the sample
 513 size of each category. Table S1 summarizes different sampling locations, sampling seasons and sampling methods observed for the
 514 investigated target compounds.

515 Another major source of uncertainty arises from the variability in sampling depths of the ULW (Table S1), which can affect
 516 the comparability of different data across multiple studies that would eventually introduce bias into the interpretation of
 517 overarching trends. Additional biases which are beyond the scope of this study include the potential influence of diurnal cycles
 518 (López-Puertas et al., 2025); OM can be rapidly removed from the SML through photochemical degradation (Obernosterer et
 519 al., 2008) and also be affected by reduced bacterial metabolism due to solar radiation (Dietz et al., 1976). Therefore, taken
 520 together, our meta-data analysis suggests that, investigating SML enrichment without accounting for these influencing factors
 521 may mask true enrichment patterns, limiting the ability to derive meaningful insights. In light of these considerations, our work
 522 highlights the need for conducting species-specific and condition-dependent analyses in future SML research that also focus
 523 on subsequent environmental parameters, as also proposed by Pereira et al. (2018).

524 4.2 Scale-related biases in EF estimates

525 Accurate data interpretation is essential to gain precise insights and arrive at substantiated conclusions (Isles, 2020; Menge et
526 al., 2018). This is particularly true for meta-analyses involving continuous environmental data where values may vary by
527 several orders of magnitude (e.g., Vitousek, 2004). In our study, when the PDF_C vs. PDF_N (Fig. 1) and PDF_D vs. PDF_P (Fig.
528 2) are evaluated on a linear scale (panels (a)), they exhibit right-skewness, whereas their log-transformed versions approximate
529 normal distributions (panels (b)). Comparisons between highly skewed distributions raise uncertainties as their offsets are
530 often dominated by extreme values/outliers. In contrast, when log transformation is applied, the distributions tend to exhibit
531 more symmetric, normalized patterns which enable direct comparisons in shape and spread across different categories (Zuur
532 et al., 2007). Therefore the normality assumption for EF is inappropriate and the computation of an arithmetic mean, a
533 conventional practice adopted in many earlier works (e.g., Gao et al., 2012; Gašparović and Čosović, 2001; Kuznetsova et al.,
534 2005; Williams et al., 1986; Wurl et al., 2009; Wurl and Holmes, 2008), can be misleading, likely providing a biased general
535 picture of OM enrichment in the SML.

536 The here constructed PDFs given in Figures 1 and 2 reveal that both mode (x_m ; shown by solid straight lines) and arithmetic
537 mean (\bar{x}_a ; shown by dashed straight lines) differ between the two scales: The mode reflects the peak of a distribution and is
538 sensitive to the shape of its respective density curve. It varies depending on whether a dataset is in ‘skewed’ linear space or
539 ‘normalized’ log space and becomes ambiguous in polymodal distributions (regardless of the scale: e.g. Fig. 3). As a
540 consequence, the mode in general provides an unreliable measure of central tendency. While the linear-arithmetic mean, which
541 is influenced by outliers, result in biases that exaggerate the corresponding central tendency, the log-arithmetic mean prevents
542 the extreme values from being dominant through balanced averaging and hence provides a reliable estimation of central
543 tendency. Nevertheless, geometric mean in linear space (\bar{x}_g ; straight lines with alternating dots and dashes) is a meaningful
544 measure given that it is equivalent to the exponential of the arithmetic mean in logarithmic space (See Eqs. (B1) and (B2)).
545 Median (\tilde{x} ; dotted straight lines), on the other hand, remains relatively consistent across both scales as it is a rank-based
546 measure of central tendency that is unaffected by the magnitude of outliers. Accordingly, we suggest that future SML
547 enrichment studies employ a logarithmic scale for data analyses, and adopt either geometric mean and/or median on linear
548 scale or arithmetic mean and/or median on logarithmic scale for reliable trend analysis.

549 Based on these new insights on scale transformations and central tendency metric considerations, we have redefined the typical
550 EF values of the studied target compounds and their degrees of spread from a meta-analytical perspective, from the estimated
551 \tilde{x} , \bar{x}_a and thresholds (i.e. UT and LT) of their PDFs (Fig. 3). To re-establish these EF ranges as generally observed estimates
552 under common conditions, the box plot method (Tukey, 1977) was applied to the data to detect and remove potentially extreme
553 EF values that rarely occur in nature. By providing these systematically derived ranges, our analysis offers a robust and
554 comprehensive reference framework, enabling future SML-based studies to consistently evaluate newly obtained EF

555 measurements, assess their position relative to typical distributions, and identify deviations that may indicate unusual
556 environmental conditions or methodological inconsistencies.

557 **4.3 Role of EF in reflecting SML enrichment**

558 While the metric of EF offers a convenient way to assess the accumulation trends in the SML and therefore serves as the basis
559 for many established insights and inferences in existing SML research (see Introduction), its ability to accurately and robustly
560 express the ‘true’ enrichment nature of the SML has constantly been a question of interest (e.g., Baastrup-Spohr and Staehr,
561 2009; Hillbricht-Ilkowska and Kostrzevska-Szlakowska, 2004; Knulst et al., 1997; Kuznetsova et al., 2004; Liss and Duce,
562 1997; Münster et al., 1998; Södergren, 1987). The EF is a ratio that expresses the ‘relative’ changes in $[C]_{\text{SML}}$ with respect to
563 $[C]_{\text{ULW}}$ (Eq. (1)), and hence is sensitive to the variations in either layer. Ideally, to effectively reflect conditions of growing
564 SML enrichment, EF values should gradually rise in response to increasing $[C]_{\text{SML}}$ and decreasing $[C]_{\text{ULW}}$, which can be visibly
565 observed for DON (Fig. 7(f)), AA (Fig. 7(g)) and CHO (Fig. 7(j)). Nevertheless, our meta-analysis highlights several
566 inconsistencies that challenge the relevance of the EF values as indicators of ‘true’ SML enrichment. For instance, on one
567 hand, similar EF values can be observed for both oligotrophic and eutrophic environments (referring to the EFs of TOC: Fig.
568 7(a)), which limits the ability to distinguish the differences in their trophic status (i.e., nutrient/productivity characteristic of
569 the water body), despite them being conspicuous in TOC’s absolute concentration range (bimodal CDFs; Fig. 4(a)). On the
570 other hand, high (low) EF values may occur under oligotrophic (eutrophic) conditions leading to over- (under-) estimation of
571 ecological setting (i.e., biological and environmental context under which SML samples were collected; Fig. 7(g)).
572 Furthermore, symmetrical changes in SML and ULW yield near-constant EF values across a wide range of concentrations
573 (Fig. 7(c)), which could cause misinterpretations in key ecosystem shifts. We have also observed consistent EF values, even
574 when SML and ULW concentrations vary over several orders of magnitudes (Figs. 6(g) – (j)), which further raise concerns
575 over the metric’s robustness. Therefore, although widely used, EF values should be interpreted with caution and, combined
576 with additional parameters that provide more accurate information about the true enrichment behaviour of the SML.

577 A complementary parameter would be the typical upper limit of a $[C]_{\text{SML}}$ distribution which may reflect the maximum
578 concentration capacity of the SML. Such a measure can serve as a robust concentration estimate of such maximum capacity if
579 approximated from a meta-data derived distribution that includes observations across all diverse environmental conditions.
580 Table 1 summarizes the upper $[C]_{\text{SML}}$ threshold estimates (i.e., UT; at 95th percentile) for the target compounds, based on their
581 CDFs (Fig. 4). Although the robustness of these values largely depends on the quality and the scope of the underlying metadata,
582 our bootstrapping approach addresses these potential limitations. Nevertheless, we acknowledge that these estimates remain
583 data-constrained and therefore can improve with the inclusion of more comprehensive, high-resolution datasets across diverse
584 environmental conditions. Measured concentrations beyond these thresholds must be considered exceptionally high and
585 warrant closer investigation to determine whether they reflect specific compounds or environmental conditions, such as
586 biogeochemical, oceanographic and weather-related factors. High concentrations of CHO ($> 50 \mu\text{mol L}^{-1}$) were reported by

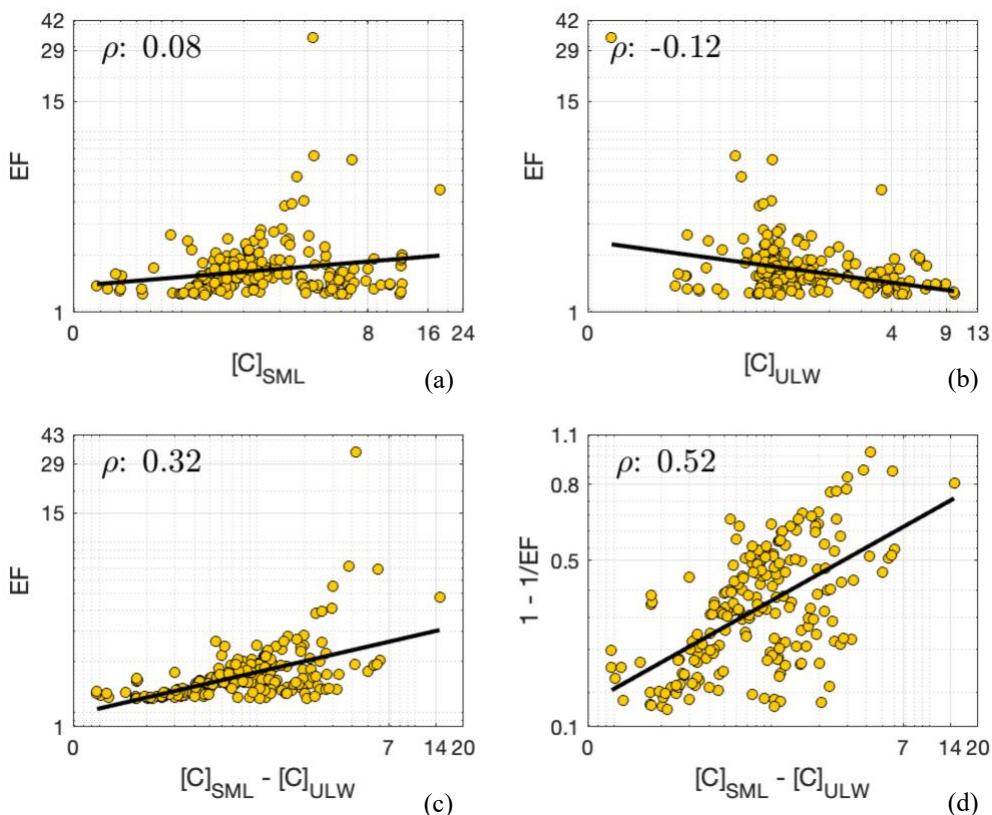
587 Milinković et al. (2022), which affect the outcome of the UT estimate. In contrast, typical CHO concentrations in the SML
 588 reported in other studies remain well below the 50 $\mu\text{mol L}^{-1}$. Since these differences cannot be resolved here, our UT estimate
 589 for CHO should therefore be treated with caution.

590 **Table 1: A summary of estimated UT values (upper threshold; concentration at 95th percentile) for [C]_{SML} distributions of the target**
 591 **compounds.** This metric represents the maximum accumulation capacity of a certain compound in the SML. The values are rounded to the
 592 nearest whole number.

Compound	TOC mg L ⁻¹	POC mg L ⁻¹	DOC mg L ⁻¹	TON mg L ⁻¹	PON mg L ⁻¹	DON mg L ⁻¹	AA $\mu\text{mol L}^{-1}$	FA $\mu\text{g L}^{-1}$	TEP $\mu\text{g Xeq L}^{-1}$	CHO $\mu\text{mol L}^{-1}$	Lipids $\mu\text{mol L}^{-1}$	Proteins $\mu\text{mol L}^{-1}$
UT value	14.0	11.0	10.0	2.0	1.0	0.5	6.0	46.0	6166.0	56.0	8.0	30.0

593 Considering absolute changes in the SML concentrations (rather than relative changes) – calculated as the magnitude difference
 594 between corresponding SML and ULW concentrations (i.e., $[\text{C}]_{\text{SML}} - [\text{C}]_{\text{ULW}}$) – provides complementary insights into the
 595 SML’s enrichment dynamics. When this metric is compared against the EF values for DOC data where $\text{EF} > \bar{x}$ ($= 1.2$), resulting
 596 Spearman’s correlation coefficients (ρ) reveal a stronger relationship (Figure 10(c); $\rho = 0.32$) relative to EF vs. $[\text{C}]_{\text{SML}}$ (Figure
 597 10(a); $\rho = 0.08$) and EF vs. $[\text{C}]_{\text{ULW}}$ (Figure 10(b); $\rho = -0.12$) correlations. This implies that although the EFs may have a limited
 598 capacity to represent the absolute concentrations of either SML or ULW, they are more responsive to the absolute concentration
 599 ‘changes’ in the two compartments. This analysis reveals that although ‘enrichment factor’ obscures accurately interpreting
 600 the trophic status or the actual enrichment in the SML, it may still hold value as a proxy that reflects the degree of partitioning
 601 between the surface microlayer and underlying waters.

602 Furthermore, normalization of $[\text{C}]_{\text{SML}} - [\text{C}]_{\text{ULW}}$ metric to the corresponding $[\text{C}]_{\text{SML}}$ values (i.e., $([\text{C}]_{\text{SML}} - [\text{C}]_{\text{ULW}})/[\text{C}]_{\text{SML}}$)
 603 ultimately yields an EF-based metric: $1 - \frac{1}{\text{EF}}$. This expresses how much of the SML concentration is above the ULW baseline,
 604 effectively providing a measure of fractional enrichment that overlooks background variability in the ULW. Unlike
 605 conventional EF values, $1 - \frac{1}{\text{EF}}$ only ranges between 0 and 1. It rescales compound-specific variability in EF and is therefore
 606 better suited for comparison across all the different observational types; normalization of EF onto a common scale allows
 607 direct evaluations without bias from different units, magnitudes or concentration ranges. This metric better captures true trends,
 608 rather than artifacts/effects of scale, while enhancing visualization and communication of results. In addition, when compared
 609 against the absolute changes, this metric exhibits stronger correlation ($\rho = 0.52$; Fig. 10(d)), likely due to increased robustness
 610 to concentration variability obtained through its scale-dependent nature. As a result, when incorporated into modelling efforts,
 611 the normalized EF metric can offer distinct advantages such as integration of heterogenous datasets, consistent
 612 parameterization, easier comparisons of model predictions and robust sensitivity analyses. Together, these benefits contribute
 613 to more reliable and generalizable models of SML processes.



614 **Figure 10: Correlations between EF and (a) $[C]_{\text{SML}}$, (b) $[C]_{\text{ULW}}$, (c) $[C]_{\text{SML}} - [C]_{\text{ULW}}$ and, (d) correlation between $1 - 1/\text{EF}$ and $[C]_{\text{SML}}$**
 615 **$- [C]_{\text{ULW}}$.** These plots were generated for DOC data, in order to investigate the observed lack of correlation among $\text{EF} - [C]_{\text{SML}} - [C]_{\text{ULW}}$,
 616 as shown by Fig. 7(c).

617 5. Conclusion

618 This study presents the first known meta-analysis of the SML, integrating a broad dataset of $[C]_{\text{SML}}$ and $[C]_{\text{ULW}}$ measurements
 619 to resolve methodological inconsistencies and establish a consensus-based understanding of SML enrichment dynamics. By
 620 meeting the statistical requirements for combining EF data and applying KDE as a robust analytical framework, we provide
 621 reliable distributional estimates and redefine typical EF ranges for 12 organic compounds, offering a comprehensive reference
 622 for assessing whether new observations fall within expected conditions or reflect unusual enrichment. Our results indicate that
 623 nitrogen-rich compounds and particulate OM exhibit stronger enrichment than carbon-rich and dissolved compounds.
 624 Nevertheless, the differing enrichment behavior of individual surfactants highlights that their surface-active properties, rather
 625 than elemental composition alone, govern overall SML enrichment. Amongst these, the fatty acids clearly show the greatest
 626 potential for high enrichment in the SML. This emphasizes the need to consider compound-specific chemistry as well as

627 environmental and methodological variability when interpreting SML processes, assessing their role in global gas flux
628 estimates and, developing models. Our assessment also inquired into the suitability of EF values as indicators of true SML
629 enrichment and suggests that, while EFs capture relative partitioning between the SML and ULW, they fall short in resolving
630 trophic variability. This study proposes complementary metrics (i.e., absolute concentration differences, SML concentration
631 capacities and fractional enrichment) that isolate true SML enrichment and support improved SML modelling. Finally, we
632 demonstrate that logarithmic transformations and robust central tendency metrics substantially improve statistical reliability
633 and data comparability over traditional linear-scale approaches, providing essential methodological guidance for future SML
634 research and its application to global air-sea exchange studies.

635 **Appendix A: KDE method – additional information**

636 Although the most basic non-parametric method to derive a probability distribution is histograms, they present two key
637 limitations for comparative studies: (1) unequal sample sizes across comparative groups restrict the use of uniform binning
638 and, (2) imposing uniform bin sizes potentially mask important distributional characteristics. In contrast, KDE circumvents
639 these issues by accounting a datapoint's exact value rather than assigning it to a particular bin of a certain width. This describes
640 the true underlying distribution of the data and allows more consistent and detailed comparisons of distributions. In this
641 analysis, we use Gaussian kernels – smooth, bell-shaped functions based on normal distribution – that weight observations
642 based on their distance. Chen (2017) and the references therein provide a comprehensive review of the KDE and its recent
643 advances.

644 In Gaussian kernels, bandwidth is analogous to standard deviation. In this study, the bandwidths for the linear KDEs were
645 computed based on an approach that includes a bias-variance trade-off. Briefly, the bias-variance trade-off represents kernels
646 that have a bandwidth that avoids too much variance in the estimates (i.e., bandwidths are not too small) while it does not
647 introduce too much bias for ranges that actually exhibit no data points (i.e., bandwidths are not too large). Calculations of
648 optimal bandwidth applied herein and an example of a bias-variance trade-off are described in Schartau et al. (2010).
649 Nevertheless, in log-space, unlike in linear-space, data are more evenly distributed and hence fixed bandwidths avoid over-
650 smoothing of low values and under-smoothing of high values.

651 The selection of an optimal bandwidth for KDEs is influenced by sample size; smaller sample sizes lead to sparse and noisy
652 distributions which require more smoothing and therefore larger bandwidths. Excessively large bandwidths can result in
653 underfitting. In contrast, larger sample sizes may allow excessively smaller bandwidths that can lead to overfitting. Bootstrap
654 resampling addresses these potential uncertainties in our analysis and, ensures the robustness and precision of the estimated
655 density distributions. Deviations between the bootstrapped KDEs and their ensemble mean were found to approximate a
656 normal distribution (consistent with Central Limit Theorem). Therefore, these ensemble means can be regarded as reliable

657 representations of the underlying data, supporting valid comparisons of probability distributions across different groups or
658 clusters.

659 **Appendix B: Mathematical expressions of distributional characteristics**

660 If a dataset contains values of ‘ x_i ’ with a sample size of ‘ n ’, mode (x_m) is the most frequently occurring value in the dataset
661 and therefore, the point where a PDF reaches its highest density. A distribution appears to be the most concentrated at x_m .
662 Median (\tilde{x}) returns the value at the 50th percentile of an ascending dataset. It divides the area under a PDF into two equal halves.
663 The arithmetic mean (\bar{x}_a), is the average of a distribution, given by the following equation:

$$664 \quad \Sigma_{i=1}^n \frac{x_i}{n} \quad (B1)$$

665 \bar{x}_a gives the point where weighted sum of a PDF is balanced. However, in the case of datasets that range over several orders
666 of magnitude, the geometric mean (hereafter referred to as ‘ \bar{x}_g ’) is the more preferred central tendency estimate, as it accounts
667 for the relative proportions of values (as opposed to their absolute magnitudes as is the case in \bar{x}_a) and hence, is less sensitive
668 to outliers. \bar{x}_g is calculated by the following equation:

$$669 \quad (\Pi_{i=1}^n x_i)^{\frac{1}{n}} \quad (B2)$$

670 \bar{x}_g of a linear distribution is mathematically equal to the exponentiated \bar{x}_a of the log-transformed version of the same
671 distribution.

672 In addition, the following equation, which accounts for the squared differences across all the datapoints of the corresponding
673 CDFs, estimates the discrete form of the integrated quadratic distance (IQD, explained in section 2.2.2), with $\Delta x_i = x_i - x_{i-1}$:

$$674 \quad IQD = \Sigma_{i=1}^n \left(\left(CDF_{[C]_{SML}(x_i)} - CDF_{[C]_{ULW}(x_i)} \right)^2 \times \Delta x_i \right) \quad (B3)$$

675 A higher IQD value implies that the divergence is greater and therefore the corresponding CDFs are more different.

676 **Code availability**

677 Computational codes used in this study are available at OceanRep GEOMAR [<https://oceanrep.geomar.de/id/eprint/63615/>].
678 The repository includes the implementation of the KDE method, representative example scripts demonstrating its application
679 for generating probability density functions and cumulative density functions, and a script to reproduce the correlation plots
680 presented.

681 **Data availability**

682 All data used in this study were extracted from previously published peer-reviewed sources and are publicly available through
683 the PANGAEA data repository [<https://doi.pangaea.de/10.1594/PANGAEA.990017>]. Full citations for all the datasets are
684 provided in supplementary information. No new data were generated for this study.

685 **Author contribution**

686 A. S. – Data Curation, Conceptualization, Methodology, Formal Analysis, Visualization, Writing – Original Draft, Writing –
687 Review & Editing

688 S. N. – Data Curation, Writing – Review & Editing

689 T. B. – Data Provision, Writing – Review & Editing

690 A. E. – Funding Acquisition, Data Provision, Writing – Review & Editing

691 H. H. – Data Provision, Writing – Review & Editing

692 M. P. – Data Provision, Writing – Review & Editing

693 K. W. – Methodology, Writing – Review & Editing

694 O. W. – Funding Acquisition, Data Provision, Writing – Review & Editing

695 M. S. – Conceptualization, Methodology, Formal Analysis, Visualization, Funding Acquisition, Supervision, Writing –
696 Review & Editing

697 **Competing interests**

698 Authors A. S., T. B., A. E. and M. S. are affiliated with the same institution as H. B., who serves as an overseeing editor for
699 the special issue “Biogeochemical processes and air-sea exchange in the sea-surface microlayer”. Authors A. S., T. B., A. E.,
700 H. H., M. P., O. W. and M. S. are collaborators with H. B. on an ongoing research project. These potential competing interests
701 have been fully disclosed to the journal. The authors declare no other competing interests relevant to the submitted work.

702 **Acknowledgements**

703 The authors gratefully acknowledge the support and collaboration of colleagues and institutions involved in this work. We also
704 acknowledge the valuable contributions of the authors of previously published datasets that were used in this study. Their work
705 provided essential input for our analysis. This study was conducted as part of the project “Biogeochemical processes and air-
706 sea exchange in the sea-surface microlayer (BASS)”, and we thank all project partners for their support and scientific exchange.

707 **Financial support**

708 This work is supported by the project “Biogeochemical processes and air-sea exchange in the sea-surface microlayer (BASS)”,
709 which is funded by the German Research Foundation (DFG) under Grant No 451574234: SCHA 2123/1-1. Data compilation
710 had been initiated through the large integrated project “Surface Ocean Processes in the Anthropocene (SOPRAN, 03F0662A)”,
711 funded by the German Federal Ministry of Education and Research (BMBF). Research contributions from M.S., A.E., and
712 K.W. were supported through the Research Program "Changing Earth - Sustaining our Future" of the Helmholtz Association.

713 **References**

714 Alldredge, A. L., Passow, U., and Logan, B. E.: The abundance and significance of a class of large, transparent organic particles
715 in the ocean, *Deep Sea Res. Part Oceanogr. Res. Pap.*, 40, 1131–1140, [https://doi.org/10.1016/0967-0637\(93\)90129-Q](https://doi.org/10.1016/0967-0637(93)90129-Q), 1993.

716 Asher, W.: The sea-surface microlayer and its effect on global air–sea gas transfer, in: *The Sea Surface and Global Change*,
717 edited by: Liss, P. S. and Duce, R. A., Cambridge University Press, 251–286,
718 <https://doi.org/10.1017/CBO9780511525025.009>, 1997.

719 Asmussen-Schäfer, F., Ribas-Ribas, M., Wurl, O., and Friedrichs, G.: Linking surface coverage with surfactant activity to
720 refine the role of surfactants for air-sea gas exchange, *EGU sphere* [preprint], <https://doi.org/10.5194/egusphere-2025-5276>,
721 19 January 2026.

722 Astrahan, P., Herut, B., Paytan, A., and Rahav, E.: The Impact of Dry Atmospheric Deposition on the Sea-Surface Microlayer
723 in the SE Mediterranean Sea: An Experimental Approach, *Front. Mar. Sci.*, 3, <https://doi.org/10.3389/fmars.2016.00222>, 2016.

724 Baastrup-Spohr, L. and Staehr, P. A.: Surface microlayers on temperate lowland lakes, *Hydrobiologia*, 625, 43–59,
725 <https://doi.org/10.1007/s10750-008-9695-3>, 2009.

726 Baier, R., DW, G., Perlmutter, S., and King, R.: Dominant chemical composition of sea-surface films, natural slicks, and
727 foams., 1974.

728 Barthelmeß, T. and Engel, A.: How biogenic polymers control surfactant dynamics in the surface microlayer: insights from a
729 coastal Baltic Sea study, *Biogeosciences*, 19, 4965–4992, <https://doi.org/10.5194/bg-19-4965-2022>, 2022.

730 Barthelmeß, T., Schütte, F., and Engel, A.: Variability of the Sea Surface Microlayer Across a Filament’s Edge and Potential
731 Influences on Gas Exchange, *Front. Mar. Sci.*, 8, 718384, <https://doi.org/10.3389/fmars.2021.718384>, 2021.

732 Brinis, A., Méjanelle, L., Momzikoff, A., Gondry, G., Fillaux, J., Point, V., and Saliot, A.: Phospholipid ester-linked fatty
733 acids composition of size-fractionated particles at the top ocean surface, *Org. Geochem.*, 35, 1275–1287,
734 <https://doi.org/10.1016/j.orggeochem.2004.04.009>, 2004.

735 Carlson, D. J.: Dissolved organic materials in surface microlayers: Temporal and spatial variability and relation to sea state,
736 *Limnol. Oceanogr.*, 28, 415–431, <https://doi.org/10.4319/lo.1983.28.3.0415>, 1983.

737 Carlucci, A. F., Craven, D. B., and Henrichs, S. M.: Surface-film microheterotrophs: amino acid metabolism and solar radiation
738 effects on their activities, *Mar. Biol.*, 85, 13–22, <https://doi.org/10.1007/BF00396410>, 1985.

- 739 Cen-Lin, H. and Tzung-May, F.: Air-Sea Exchange of Volatile Organic Compounds: A New Model with Microlayer Effects,
740 Atmospheric Ocean. Sci. Lett., 6, 97–102, <https://doi.org/10.1080/16742834.2013.11447063>, 2013.
- 741 Chen, Y., Yang, G.-P., Xia, Q.-Y., and Wu, G.-W.: Enrichment and characterization of dissolved organic matter in the surface
742 microlayer and subsurface water of the South Yellow Sea, Mar. Chem., 182, 1–13,
743 <https://doi.org/10.1016/j.marchem.2016.04.001>, 2016.
- 744 Chen, Y.-C.: A tutorial on kernel density estimation and recent advances, Biostat. Epidemiol., 1, 161–187,
745 <https://doi.org/10.1080/24709360.2017.1396742>, 2017.
- 746 Čosović, B. and Vojvodić, V.: Adsorption behaviour of the hydrophobic fraction of organic matter in natural waters, Mar.
747 Chem., 28, 183–198, [https://doi.org/10.1016/0304-4203\(89\)90194-1](https://doi.org/10.1016/0304-4203(89)90194-1), 1989.
- 748 Čosović, B. and Vojvodić, V.: Voltammetric Analysis of Surface Active Substances in Natural Seawater, Electroanalysis, 10,
749 429–434, [https://doi.org/10.1002/\(SICI\)1521-4109\(199805\)10:6%253C429::AID-ELAN429%253E3.0.CO;2-7](https://doi.org/10.1002/(SICI)1521-4109(199805)10:6%253C429::AID-ELAN429%253E3.0.CO;2-7), 1998.
- 750 Crocetti, E.: Systematic Reviews With Meta-Analysis: Why, When, and How?, Emerg. Adulthood, 4, 3–18,
751 <https://doi.org/10.1177/2167696815617076>, 2016.
- 752 Cunliffe, M. and Murrell, J. C.: The sea-surface microlayer is a gelatinous biofilm, ISME J., 3, 1001–1003,
753 <https://doi.org/10.1038/ismej.2009.69>, 2009.
- 754 Cunliffe, M., Salter, M., Mann, P. J., Whiteley, A. S., Upstill-Goddard, R. C., and Murrell, J. C.: Dissolved organic carbon
755 and bacterial populations in the gelatinous surface microlayer of a Norwegian fjord mesocosm, FEMS Microbiol. Lett., 299,
756 248–254, <https://doi.org/10.1111/j.1574-6968.2009.01751.x>, 2009.
- 757 Cunliffe, M., Engel, A., Frka, S., Gašparović, B., Guitart, C., Murrell, J. C., Salter, M., Stolle, C., Upstill-Goddard, R., and
758 Wurl, O.: Sea surface microlayers: A unified physicochemical and biological perspective of the air–ocean interface, Prog.
759 Oceanogr., 109, 104–116, <https://doi.org/10.1016/j.pocean.2012.08.004>, 2013.
- 760 Dietz, A. S., Albright, L. J., and Tuominen, T.: Heterotrophic activities of bacterioneuston and bacterioplankton, Can. J.
761 Microbiol., 22, 1699–1709, <https://doi.org/10.1139/m76-251>, 1976.
- 762 Dukhin, S. S., Kovalchuk, V. I., Gochev, G. G., Lotfi, M., Krzan, M., Malysa, K., and Miller, R.: Dynamics of Rear Stagnant
763 Cap formation at the surface of spherical bubbles rising in surfactant solutions at large Reynolds numbers under conditions of
764 small Marangoni number and slow sorption kinetics, Adv. Colloid Interface Sci., 222, 260–274,
765 <https://doi.org/10.1016/j.cis.2014.10.002>, 2015.
- 766 Engel, A. and Galgani, L.: The organic sea-surface microlayer in the upwelling region off the coast of Peru and potential
767 implications for air–sea exchange processes, Biogeosciences, 13, 989–1007, <https://doi.org/10.5194/bg-13-989-2016>, 2016.
- 768 Engel, A., Thoms, S., Riebesell, U., Rochelle-Newall, E., and Zondervan, I.: Polysaccharide aggregation as a potential sink of
769 marine dissolved organic carbon, Nature, 428, 929–932, <https://doi.org/10.1038/nature02453>, 2004.
- 770 Engel, A., Bange, H. W., Cunliffe, M., Burrows, S. M., Friedrichs, G., Galgani, L., Herrmann, H., Hertkorn, N., Johnson, M.,
771 Liss, P. S., Quinn, P. K., Schartau, M., Soloviev, A., Stolle, C., Upstill-Goddard, R. C., Van Pinxteren, M., and Zäncker, B.:
772 The Ocean’s Vital Skin: Toward an Integrated Understanding of the Sea Surface Microlayer, Front. Mar. Sci., 4, 165,
773 <https://doi.org/10.3389/fmars.2017.00165>, 2017.

- 774 Feenstra, S.: Use of Logarithmic-Scale Correlation Plots to Represent Contaminant Ratios for Evaluation of Subsurface
775 Environmental Data, *Environ. Forensics*, 7, 175–185, <https://doi.org/10.1080/15275920600667153>, 2006.
- 776 Frew, N. M.: The role of organic films in air–sea gas exchange, in: *The Sea Surface and Global Change*, edited by: Liss, P. S.
777 and Duce, R. A., Cambridge University Press, Cambridge, 121–172, <https://doi.org/10.1017/CBO9780511525025.006>, 1997.
- 778 Frew, N. M., Bock, E. J., Schimpf, U., Hara, T., Haußecker, H., Edson, J. B., McGillis, W. R., Nelson, R. K., McKenna, S. P.,
779 Uz, B. M., and Jähne, B.: Air-sea gas transfer: Its dependence on wind stress, small-scale roughness, and surface films, *J.*
780 *Geophys. Res. Oceans*, 109, 2003JC002131, <https://doi.org/10.1029/2003JC002131>, 2004.
- 781 Frka, S., Pogorzelski, S., Kozarac, Z., and Čosović, B.: Physicochemical Signatures of Natural Sea Films from Middle Adriatic
782 Stations, *J. Phys. Chem. A*, 116, 6552–6559, <https://doi.org/10.1021/jp212430a>, 2012.
- 783 Gao, Q., Leck, C., Rauschenberg, C., and Matrai, P. A.: On the chemical dynamics of extracellular polysaccharides in the high
784 Arctic surface microlayer, *Ocean Sci.*, 8, 401–418, <https://doi.org/10.5194/os-8-401-2012>, 2012.
- 785 Garabetian, F., Romano, J.-C., Paul, R., and Sigoillot, J.-C.: Organic matter composition and pollutant enrichment of sea
786 surface microlayer inside and outside slicks, *Mar. Environ. Res.*, 35, 323–339, [https://doi.org/10.1016/0141-1136\(93\)90100-](https://doi.org/10.1016/0141-1136(93)90100-)
787 E, 1993.
- 788 Gašparović, B. and Čosović, B.: Distribution of surface-active substances in the northern Adriatic Sea, *Mar. Chem.*, 75, 301–
789 313, [https://doi.org/10.1016/S0304-4203\(01\)00044-5](https://doi.org/10.1016/S0304-4203(01)00044-5), 2001.
- 790 Gašparović, B. and Čosović, B.: Surface-active properties of organic matter in the North Adriatic Sea, *Estuar. Coast. Shelf*
791 *Sci.*, 58, 555–566, [https://doi.org/10.1016/S0272-7714\(03\)00133-1](https://doi.org/10.1016/S0272-7714(03)00133-1), 2003.
- 792 Gašparović, B., Plavšić, M., Čosović, B., and Saliot, A.: Organic matter characterization in the sea surface microlayers in the
793 subarctic Norwegian fjords region, *Mar. Chem.*, 105, 1–14, <https://doi.org/10.1016/j.marchem.2006.12.010>, 2007.
- 794 Goldman, J. C., Dennett, M. R., and Frew, N. M.: Surfactant effects on air-sea gas exchange under turbulent conditions, *Deep*
795 *Sea Res. Part Oceanogr. Res. Pap.*, 35, 1953–1970, [https://doi.org/10.1016/0198-0149\(88\)90119-7](https://doi.org/10.1016/0198-0149(88)90119-7), 1988.
- 796 Härdle, W., Werwatz, A., Müller, M., and Sperlich, S.: *Nonparametric and Semiparametric Models*, Springer Berlin
797 Heidelberg, Berlin, Heidelberg, <https://doi.org/10.1007/978-3-642-17146-8>, 2004.
- 798 Harvey, H. R., Tuttle, J. H., and Bell, J. T.: Kinetics of phytoplankton decay during simulated sedimentation: Changes in
799 biochemical composition and microbial activity under oxic and anoxic conditions, *Geochim. Cosmochim. Acta*, 59, 3367–
800 3377, [https://doi.org/10.1016/0016-7037\(95\)00217-N](https://doi.org/10.1016/0016-7037(95)00217-N), 1995.
- 801 Hedges, J. I., Cowie, G. L., Richey, J. E., Quay, P. D., Benner, R., Strom, M., and Forsberg, B. R.: Origins and processing of
802 organic matter in the Amazon River as indicated by carbohydrates and amino acids, *Limnol. Oceanogr.*, 39, 743–761,
803 <https://doi.org/10.4319/lo.1994.39.4.0743>, 1994.
- 804 Henrichs, S. M. and Williams, P. M.: Dissolved and particulate amino acids and carbohydrates in the sea surface microlayer,
805 *Mar. Chem.*, 17, 141–163, [https://doi.org/10.1016/0304-4203\(85\)90070-2](https://doi.org/10.1016/0304-4203(85)90070-2), 1985.
- 806 Hillbricht-Ilkowska, A. and Kostrzewska-Szlakowska, I.: Surface microlayer in lakes of different trophic status: nutrients
807 concentration and accumulation, *Pol. J. Ecol.*, 52, 461–478, 2004.

- 808 Hunter, K. A.: Processes affecting particulate trace metals in the sea surface microlayer, *Mar. Chem.*, 9, 49–70,
809 [https://doi.org/10.1016/0304-4203\(80\)90006-7](https://doi.org/10.1016/0304-4203(80)90006-7), 1980.
- 810 Hunter, K. A. and Liss, P. S.: The input of organic material to the oceans: air—sea interactions and the organic chemical
811 composition of the sea surface, *Mar. Chem.*, 5, 361–379, [https://doi.org/10.1016/0304-4203\(77\)90029-9](https://doi.org/10.1016/0304-4203(77)90029-9), 1977.
- 812 Hunter, K. A. and Liss, P. S.: Chapter 9 Organic Sea Surface Films, in: Elsevier Oceanography Series, vol. 31, edited by:
813 Duursma, E. K. and Dawson, R., Elsevier, 259–298, [https://doi.org/10.1016/S0422-9894\(08\)70331-3](https://doi.org/10.1016/S0422-9894(08)70331-3), 1981.
- 814 Isles, P. D. F.: The misuse of ratios in ecological stoichiometry, *Ecology*, 101, e03153, <https://doi.org/10.1002/ecy.3153>, 2020.
- 815 Jørgensen, N., Kroer, N., Coffin, R., Yang, X.-H., and Lee, C.: Dissolved free amino acids, combined amino acids, and DNA
816 as sources of carbon and nitrogen to marine bacteria, *Mar. Ecol. Prog. Ser.*, 98, 135–148, <https://doi.org/10.3354/meps098135>,
817 1993.
- 818 Joux, F., Agogué, H., Obernosterer, I., Dupuy, C., Reinthaler, T., Herndl, G., and Lebaron, P.: Microbial community structure
819 in the sea surface microlayer at two contrasting coastal sites in the northwestern Mediterranean Sea, *Aquat. Microb. Ecol.*, 42,
820 91–104, <https://doi.org/10.3354/ame042091>, 2006.
- 821 Keene, O. N.: The log transformation is special, *Stat. Med.*, 14, 811–819, <https://doi.org/10.1002/sim.4780140810>, 1995.
- 822 Kjelleberg, S., Norkrans, B., Löfgren, H., and Larsson, K.: Surface balance study of the interaction between microorganisms
823 and lipid monolayer at the air/water interface, *Appl. Environ. Microbiol.*, 31, 609–611, <https://doi.org/10.1128/aem.31.4.609->
824 [611.1976](https://doi.org/10.1128/aem.31.4.609-611.1976), 1976.
- 825 Knipping, E. M., Lakin, M. J., Foster, K. L., Jungwirth, P., Tobias, D. J., Gerber, R. B., Dabdub, D., and Finlayson-Pitts, B.
826 J.: Experiments and Simulations of Ion-Enhanced Interfacial Chemistry on Aqueous NaCl Aerosols, *Science*, 288, 301–306,
827 <https://doi.org/10.1126/science.288.5464.301>, 2000.
- 828 Knulst, J. C., Backlund, P., Hessen, D. O., Riise, G., and Södergren, A.: Response of surface microlayers to artificial acid
829 precipitation in a meso-humic lake in Norway, *Water Res.*, 31, 2177–2186, [https://doi.org/10.1016/S0043-1354\(97\)00061-4](https://doi.org/10.1016/S0043-1354(97)00061-4),
830 1997.
- 831 Kock, A., Schafstall, J., Dengler, M., Brandt, P., and Bange, H. W.: Sea-to-air and diapycnal nitrous oxide fluxes in the eastern
832 tropical North Atlantic Ocean, *Biogeosciences*, 9, 957–964, <https://doi.org/10.5194/bg-9-957-2012>, 2012.
- 833 Kujawinski, E. B., Farrington, J. W., and Moffett, J. W.: Evidence for grazing-mediated production of dissolved surface-active
834 material by marine protists, *Mar. Chem.*, 77, 133–142, [https://doi.org/10.1016/S0304-4203\(01\)00082-2](https://doi.org/10.1016/S0304-4203(01)00082-2), 2002.
- 835 Kurata, N., Vella, K., Hamilton, B., Shivji, M., Soloviev, A., Matt, S., Tartar, A., and Perrie, W.: Surfactant-associated bacteria
836 in the near-surface layer of the ocean, *Sci. Rep.*, 6, 19123, <https://doi.org/10.1038/srep19123>, 2016.
- 837 Kuznetsova, M. and Lee, C.: Dissolved free and combined amino acids in nearshore seawater, sea surface microlayers and
838 foams: Influence of extracellular hydrolysis, *Aquat. Sci.*, 64, 252–268, <https://doi.org/10.1007/s00027-002-8070-0>, 2002.
- 839 Kuznetsova, M., Lee, C., Aller, J., and Frew, N.: Enrichment of amino acids in the sea surface microlayer at coastal and open
840 ocean sites in the North Atlantic Ocean, *Limnol. Oceanogr.*, 49, 1605–1619, <https://doi.org/10.4319/lo.2004.49.5.1605>, 2004.
- 841 Kuznetsova, M., Lee, C., and Aller, J.: Characterization of the proteinaceous matter in marine aerosols, *Mar. Chem.*, 96, 359–
842 377, <https://doi.org/10.1016/j.marchem.2005.03.007>, 2005.

- 843 Laß, K. and Friedrichs, G.: Revealing structural properties of the marine nanolayer from vibrational sum frequency generation
844 spectra, *J. Geophys. Res.*, 116, C08042, <https://doi.org/10.1029/2010JC006609>, 2011.
- 845 Laß, K., Bange, H. W., and Friedrichs, G.: Seasonal signatures in SFG vibrational spectra of the sea surface nanolayer at
846 Boknis Eck Time Series Station (SW Baltic Sea), *Biogeosciences*, 10, 5325–5334, <https://doi.org/10.5194/bg-10-5325-2013>,
847 2013.
- 848 Li, L., Wu, P., Zhang, P., Huang, S., and Zhang, Y.: An improved model for air–sea exchange of elemental mercury in
849 MITgcm-ECCOV4-Hg: the role of surfactants and waves, *Geosci. Model Dev.*, 17, 8683–8695, <https://doi.org/10.5194/gmd-17-8683-2024>, 2024.
- 850
- 851 Liss, P. S. and Duce, R. A.: *The sea surface and global change*, Cambridge University Press, 535 pp., 1997.
- 852 Liu, K. and Dickhut, R. M.: Effects of wind speed and particulate matter source on surface microlayer characteristics and
853 enrichment of organic matter in southern Chesapeake Bay, *J. Geophys. Res. Atmospheres*, 103, 10571–10577,
854 <https://doi.org/10.1029/97JD03736>, 1998.
- 855 López-Puertas, A., Wurl, O., Frka, S., and Ribas-Ribas, M.: Diel Variability Affects the Inorganic Marine Carbon System in
856 the Sea-Surface Microlayer of a Mediterranean coastal area (Šibenik, Croatia), *EGUsphere* [preprint],
857 <https://doi.org/10.5194/egusphere-2025-2090>, 16 May 2025.
- 858 MacIntyre, F.: Chemical fractionation and sea-surface microlayer processes, *The sea*, 5, 245–299, 1974.
- 859 Maki, J. S. and Hermansson, M.: The dynamics of surface microlayers in aquatic environments, *Biol. Part. Aquat. Syst. Second*
860 *Ed.*, 161–182, 2020.
- 861 Mari, X. and Burd, A.: Seasonal size spectra of transparent exopolymeric particles (TEP) in a coastal sea and comparison with
862 those predicted using coagulation theory, *Mar. Ecol. Prog. Ser.*, 163, 63–76, <https://doi.org/10.3354/meps163063>, 1998.
- 863 Mari, X., Passow, U., Migon, C., Burd, A. B., and Legendre, L.: Transparent exopolymer particles: Effects on carbon cycling
864 in the ocean, *Prog. Oceanogr.*, 151, 13–37, <https://doi.org/10.1016/j.pocean.2016.11.002>, 2017.
- 865 Marty, J. C. and Saliot, A.: Hydrocarbons (normal alkanes) in the surface microlayer of seawater, *Deep Sea Res. Oceanogr.*
866 *Abstr.*, 23, 863–873, [https://doi.org/10.1016/0011-7471\(76\)90853-6](https://doi.org/10.1016/0011-7471(76)90853-6), 1976.
- 867 McKenna, S. P. and McGillis, W. R.: The role of free-surface turbulence and surfactants in air–water gas transfer, *Int. J. Heat*
868 *Mass Transf.*, 47, 539–553, <https://doi.org/10.1016/j.ijheatmasstransfer.2003.06.001>, 2004.
- 869 Menge, D. N. L., MacPherson, A. C., Bytnerowicz, T. A., Quebbeman, A. W., Schwartz, N. B., Taylor, B. N., and Wolf, A.
870 A.: Logarithmic scales in ecological data presentation may cause misinterpretation, *Nat. Ecol. Evol.*, 2, 1393–1402,
871 <https://doi.org/10.1038/s41559-018-0610-7>, 2018.
- 872 Mengist, W., Soromessa, T., and Legese, G.: Method for conducting systematic literature review and meta-analysis for
873 environmental science research, *MethodsX*, 7, 100777, <https://doi.org/10.1016/j.mex.2019.100777>, 2020.
- 874 Milinković, A., Penezić, A., Kušan, A. C., Gluščić, V., Žužul, S., Skejić, S., Šantić, D., Godec, R., Pehnec, G., Omanović, D.,
875 Engel, A., and Frka, S.: Variabilities of biochemical properties of the sea surface microlayer: Insights to the atmospheric
876 deposition impacts, *Sci. Total Environ.*, 838, 156440, <https://doi.org/10.1016/j.scitotenv.2022.156440>, 2022.

- 877 Mopper, K., Zhou, J., Sri Ramana, K., Passow, U., Dam, H. G., and Drapeau, D. T.: The role of surface-active carbohydrates
878 in the flocculation of a diatom bloom in a mesocosm, *Deep Sea Res. Part II Top. Stud. Oceanogr.*, 42, 47–73,
879 [https://doi.org/10.1016/0967-0645\(95\)00004-A](https://doi.org/10.1016/0967-0645(95)00004-A), 1995.
- 880 Münster, U., Heikkinen, E., and Knulst, J.: Nutrient composition, microbial biomass and activity at the air-water interface of
881 small boreal forest lakes, in: *Eutrophication in Planktonic Ecosystems: Food Web Dynamics and Elemental Cycling*, edited
882 by: Tamminen, T. and Kuosa, H., Springer Netherlands, Dordrecht, 261–270, https://doi.org/10.1007/978-94-017-1493-8_21,
883 1998.
- 884 Mustaffa, N. I. H., Badewien, T. H., Ribas-Ribas, M., and Wurl, O.: High-resolution observations on enrichment processes in
885 the sea-surface microlayer, *Sci. Rep.*, 8, 13122, <https://doi.org/10.1038/s41598-018-31465-8>, 2018.
- 886 Mustaffa, N. I. H., Ribas-Ribas, M., Banko-Kubis, H. M., and Wurl, O.: Global reduction of *in situ* CO₂ transfer velocity by
887 natural surfactants in the sea-surface microlayer, *Proc. R. Soc. Math. Phys. Eng. Sci.*, 476, 20190763,
888 <https://doi.org/10.1098/rspa.2019.0763>, 2020.
- 889 Myklestad, S. M.: Release of extracellular products by phytoplankton with special emphasis on polysaccharides, *Sci. Total*
890 *Environ.*, 165, 155–164, [https://doi.org/10.1016/0048-9697\(95\)04549-G](https://doi.org/10.1016/0048-9697(95)04549-G), 1995.
- 891 Obernosterer, I., Catala, P., Reinthaler, T., Herndl, G., and Lebaron, P.: Enhanced heterotrophic activity in the surface
892 microlayer of the Mediterranean Sea, *Aquat. Microb. Ecol.*, 39, 293–302, <https://doi.org/10.3354/ame039293>, 2005.
- 893 Obernosterer, I., Catala, P., Lami, R., Caparros, J., Ras, J., Bricaud, A., Dupuy, C., Van Wambeke, F., and Lebaron, P.:
894 Biochemical characteristics and bacterial community structure of the sea surface microlayer in the South Pacific Ocean,
895 *Biogeosciences*, 5, 693–705, <https://doi.org/10.5194/bg-5-693-2008>, 2008.
- 896 Parzen, E.: On Estimation of a Probability Density Function and Mode, *Ann. Math. Stat.*, 33, 1065–1076, 1962.
- 897 Passow, U.: Formation of transparent exopolymer particles, TEP, from dissolved precursor material, *Mar. Ecol. Prog. Ser.*,
898 192, 1–11, <https://doi.org/10.3354/meps192001>, 2000.
- 899 Passow, U. and Alldredge, A. L.: Do transparent exopolymer particles (TEP) inhibit grazing by the euphausiid *Euphausia*
900 *pacifica*?, *J. Plankton Res.*, 21, 2203–2217, <https://doi.org/10.1093/plankt/21.11.2203>, 1999.
- 901 Penezić, A., Drozdowska, V., Novak, T., and Gašparović, B.: Distribution and characterization of organic matter within the
902 sea surface microlayer in the Gulf of Gdańsk, *Oceanologia*, 64, 631–650, <https://doi.org/10.1016/j.oceano.2022.05.003>, 2022.
- 903 Penna, A.: Influence of nutrient ratios on the *in vitro* extracellular polysaccharide production by marine diatoms from the
904 Adriatic Sea, *J. Plankton Res.*, 21, 1681–1690, <https://doi.org/10.1093/plankt/21.9.1681>, 1999.
- 905 Pereira, R., Schneider-Zapp, K., and Upstill-Goddard, R. C.: Surfactant control of gas transfer velocity along an offshore
906 coastal transect: results from a laboratory gas exchange tank, *Biogeosciences*, 13, 3981–3989, <https://doi.org/10.5194/bg-13-3981-2016>, 2016.
- 908 Pereira, R., Ashton, I., Sabbaghzadeh, B., Shutler, J. D., and Upstill-Goddard, R. C.: Reduced air–sea CO₂ exchange in the
909 Atlantic Ocean due to biological surfactants, *Nat. Geosci.*, 11, 492–496, <https://doi.org/10.1038/s41561-018-0136-2>, 2018.
- 910 Petersen, M. K., Iyengar, S. S., Day, T. J. F., and Voith, G. A.: The Hydrated Proton at the Water Liquid/Vapor Interface, *J.*
911 *Phys. Chem. B*, 108, 14804–14806, <https://doi.org/10.1021/jp046716o>, 2004.

- 912 Pogorzelski, S. J., Kogut, A. D., and Mazurek, A. Z.: Surface Rheology Parameters of Source-Specific Surfactant Films as
913 Indicators of Organic Matter Dynamics, *Hydrobiologia*, 554, 67–81, <https://doi.org/10.1007/s10750-005-1007-6>, 2006.
- 914 Reinthaler, T., Sintes, E., and Herndl, G. J.: Dissolved organic matter and bacterial production and respiration in the sea-
915 surface microlayer of the open Atlantic and the western Mediterranean Sea, *Limnol. Oceanogr.*, 53, 122–136,
916 <https://doi.org/10.4319/lo.2008.53.1.0122>, 2008.
- 917 Robinson, T., Wurl, O., Bahlmann, E., Jürgens, K., and Stolle, C.: Rising bubbles enhance the gelatinous nature of the air–sea
918 interface, *Limnol. Oceanogr.*, 64, 2358–2372, <https://doi.org/10.1002/lno.11188>, 2019.
- 919 Sabbaghzadeh, B., Upstill-Goddard, R. C., Beale, R., Pereira, R., and Nightingale, P. D.: The Atlantic Ocean surface
920 microlayer from 50°N to 50°S is ubiquitously enriched in surfactants at wind speeds up to 13 m s⁻¹, *Geophys. Res. Lett.*, 44,
921 2852–2858, <https://doi.org/10.1002/2017GL072988>, 2017.
- 922 Salter, M. E., Upstill-Goddard, R. C., Nightingale, P. D., Archer, S. D., Blomquist, B., Ho, D. T., Huebert, B., Schlosser, P.,
923 and Yang, M.: Impact of an artificial surfactant release on air-sea gas fluxes during Deep Ocean Gas Exchange Experiment II,
924 *J. Geophys. Res. Oceans*, 116, 2011JC007023, <https://doi.org/10.1029/2011JC007023>, 2011.
- 925 Schartau, M., Engel, A., Schröter, J., Thoms, S., Völker, C., and Wolf-Gladrow, D.: Modelling carbon overconsumption and
926 the formation of extracellular particulate organic carbon, *Biogeosciences*, 4, 433–454, <https://doi.org/10.5194/bg-4-433-2007>,
927 2007.
- 928 Schartau, M., Landry, M. R., and Armstrong, R. A.: Density estimation of plankton size spectra: a reanalysis of IronEx II data,
929 *J. Plankton Res.*, 32, 1167–1184, <https://doi.org/10.1093/plankt/fbq072>, 2010.
- 930 Shine, J. P. and Wallace, G. T.: Flux of surface-active organic complexes of copper to the air-sea interface in coastal marine
931 waters, *J. Geophys. Res. Oceans*, 101, 12017–12026, <https://doi.org/10.1029/96JC00616>, 1996.
- 932 Sieburth, J. McN.: Microbiological and Organic-Chemical Processes in the Surface and Mixed Layers, in: *Air-Sea Exchange*
933 *of Gases and Particles*, edited by: Liss, P. S. and Slinn, W. G. N., Springer Netherlands, Dordrecht, 121–172,
934 https://doi.org/10.1007/978-94-009-7169-1_3, 1983.
- 935 Sieburth, J. McN., Willis, P.-J., Johnson, K. M., Burney, C. M., Lavoie, D. M., Hinga, K. R., Caron, D. A., French, F. W.,
936 Johnson, P. W., and Davis, P. G.: Dissolved Organic Matter and Heterotrophic Microneuston in the Surface Microlayers of
937 the North Atlantic, *Science*, 194, 1415–1418, <https://doi.org/10.1126/science.194.4272.1415>, 1976.
- 938 Silverman, B. W.: *Density Estimation for Statistics and Data Analysis*, 1st ed., Routledge,
939 <https://doi.org/10.1201/9781315140919>, 2018.
- 940 Södergren, A.: Origin and composition of surface slicks in lakes of differing trophic status1, *Limnol. Oceanogr.*, 32, 1307–
941 1316, <https://doi.org/10.4319/lo.1987.32.6.1307>, 1987.
- 942 Springer, T. G. and Pigford, R. L.: Influence of Surface Turbulence and Surfactants on Gas Transport through Liquid
943 Interfaces, *Ind. Eng. Chem. Fundam.*, 9, 458–465, <https://doi.org/10.1021/i160035a025>, 1970.
- 944 Sun, C.-C., Sperling, M., and Engel, A.: Effect of wind speed on the size distribution of gel particles in the sea surface
945 microlayer: insights from a wind–wave channel experiment, *Biogeosciences*, 15, 3577–3589, <https://doi.org/10.5194/bg-15-3577-2018>, 2018.

- 947 Thornton, D. C. O., Brooks, S. D., and Chen, J.: Protein and Carbohydrate Exopolymer Particles in the Sea Surface Microlayer
948 (SML), *Front. Mar. Sci.*, 3, <https://doi.org/10.3389/fmars.2016.00135>, 2016.
- 949 Tsai, W. and Liu, K.: An assessment of the effect of sea surface surfactant on global atmosphere-ocean CO₂ flux, *J. Geophys.*
950 *Res. Oceans*, 108, 2000JC000740, <https://doi.org/10.1029/2000JC000740>, 2003.
- 951 Tukey, J. W.: *Exploratory data analysis*, Springer, 1977.
- 952 Upstill-Goddard, R. C.: Air–sea gas exchange in the coastal zone, *Estuar. Coast. Shelf Sci.*, 70, 388–404,
953 <https://doi.org/10.1016/j.ecss.2006.05.043>, 2006.
- 954 Verdugo, P., Alldredge, A. L., Azam, F., Kirchman, D. L., Passow, U., and Santschi, P. H.: The oceanic gel phase: a bridge in
955 the DOM–POM continuum, *Mar. Chem.*, 92, 67–85, <https://doi.org/10.1016/j.marchem.2004.06.017>, 2004.
- 956 Vitousek, P. M.: *Nutrient cycling and limitation: Hawai'i as a model system*, Princeton University Press, Princeton, New
957 Jersey ; Oxford, 1 pp., 2004.
- 958 Wegman, E. J.: Nonparametric probability density estimation, *J. Stat. Comput. Simul.*, 1, 225–245,
959 <https://doi.org/10.1080/00949657208810017>, 1972.
- 960 Williams, P. M., Carlucci, A. F., Henrichs, S. M., Van Vleet, E. S., Horrigan, S. G., Reid, F. M. H., and Robertson, K. J.:
961 Chemical and microbiological studies of sea-surface films in the Southern Gulf of California and off the West Coast of Baja
962 California, *Mar. Chem.*, 19, 17–98, [https://doi.org/10.1016/0304-4203\(86\)90033-2](https://doi.org/10.1016/0304-4203(86)90033-2), 1986.
- 963 Wurl, O. and Holmes, M.: The gelatinous nature of the sea-surface microlayer, *Mar. Chem.*, 110, 89–97,
964 <https://doi.org/10.1016/j.marchem.2008.02.009>, 2008.
- 965 Wurl, O., Miller, L., Röttgers, R., and Vagle, S.: The distribution and fate of surface-active substances in the sea-surface
966 microlayer and water column, *Mar. Chem.*, 115, 1–9, <https://doi.org/10.1016/j.marchem.2009.04.007>, 2009.
- 967 Wurl, O., Wurl, E., Miller, L., Johnson, K., and Vagle, S.: Formation and global distribution of sea-surface microlayers,
968 *Biogeosciences*, 8, 121–135, <https://doi.org/10.5194/bg-8-121-2011>, 2011.
- 969 Wurl, O., Stolle, C., Van Thuoc, C., The Thu, P., and Mari, X.: Biofilm-like properties of the sea surface and predicted effects
970 on air–sea CO₂ exchange, *Prog. Oceanogr.*, 144, 15–24, <https://doi.org/10.1016/j.pocan.2016.03.002>, 2016.
- 971 Yang, G.-P.: Dimethylsulfide enrichment in the surface microlayer of the South China Sea, *Mar. Chem.*, 66, 215–224,
972 [https://doi.org/10.1016/S0304-4203\(99\)00042-0](https://doi.org/10.1016/S0304-4203(99)00042-0), 1999.
- 973 Zhang, Z., Liu, C., and Liu, L.: Physicochemical Studies of the Sea-Surface Microlayer, *Front. Chem. China*, 1,
974 <https://doi.org/10.1007/s11458-005-0003-8>, 2006.
- 975 Zhou, J., Mopper, K., and Passow, U.: The role of surface-active carbohydrates in the formation of transparent exopolymer
976 particles by bubble adsorption of seawater, *Limnol. Oceanogr.*, 43, 1860–1871, <https://doi.org/10.4319/lo.1998.43.8.1860>,
977 1998.
- 978 Žutić, V., Čosović, B., Marčenko, E., Bihari, N., and Kršinić, F.: Surfactant production by marine phytoplankton, *Mar. Chem.*,
979 10, 505–520, [https://doi.org/10.1016/0304-4203\(81\)90004-9](https://doi.org/10.1016/0304-4203(81)90004-9), 1981.

980 Zuur, A. F., Ieno, E. N., and Smith, G. M. (Eds.): Linear regression, in: *Analysing Ecological Data*, Springer New York, New
981 York, NY, 49–77, https://doi.org/10.1007/978-0-387-45972-1_5, 2007.